JACS
JOURNAL OF THE AMERICAN CHEMICAL SOCIETY
pubs.acs.org/JACS
Article

In Situ Structural Observation of a Substrate- and Peroxide-Bound High-Spin Ferric-Hydroperoxo Intermediate in the P450 Enzyme CYP121

Romie C. Nguyen, Ian Davis, Medhanjali Dasgupta, Yifan Wang, Philipp S. Simon, Agata Butryn, Hiroki Makita, Isabel Bogacz, Kednerlin Dornevil, Pierre Aller, Asmit Bhowmick, Ruchira Chatterjee, In-Sik Kim, Tiankun Zhou, Derek Mendez, Daniel W. Paley, Franklin Fuller, Roberto Alonso Mori, Alexander Batyuk, Nicholas K. Sauter, Aaron S. Brewster, Allen M. Orville, Vittal K. Yachandra, Junko Yano, Jan F. Kern,* and Aimin Liu*

Cite This: J. Am. Chem. Soc. 2023, 145, 25120−25133

ABSTRACT: The P450 enzyme CYP121 from *Mycobacterium tuberculosis* catalyzes a carbon−carbon (C−C) bond coupling cyclization of the dityrosine substrate containing a diketopiperazine ring, *cyclo*(L-tyrosine-L-tyrosine) (cYY). An unusual high-spin (S = 5/2) ferric intermediate maximizes its population in less than 5 ms in the rapid freeze-quenching study of CYP121 during the shunt reaction with peracetic acid or hydrogen peroxide in acetic acid solution. We show that this intermediate can also be observed in the crystalline state by EPR spectroscopy. By developing an on-demand-rapid-mixing method for time-resolved serial femtosecond crystallography with X-ray free-electron laser (tr-SFX-XFEL) technology covering the millisecond time domain and without freezing, we structurally monitored the reaction in situ at room temperature. After a 200 ms peracetic acid reaction with the cocrystallized enzyme−substrate microcrystal slurry, a ferric-hydroperoxo intermediate is observed, and its structure is determined at 1.85 Å resolution. The structure shows a hydroperoxyl ligand between the heme and the native substrate, cYY. The oxygen atoms of the hydroperoxo are 2.5 and 3.2 Å from the iron ion. The end-on binding ligand adopts a near-side-on geometry and is weakly associated with the iron ion, causing the unusual high-spin state. This compound 0 intermediate, spectroscopically and structurally observed during the catalytic shunt pathway, reveals a unique binding mode that deviates from the end-on compound 0 intermediates in other heme enzymes. The hydroperoxyl ligand is only 2.9 Å from the bound cYY, suggesting an active oxidant role of the intermediate for direct substrate oxidation in the nonhydroxylation C−C bond coupling chemistry.

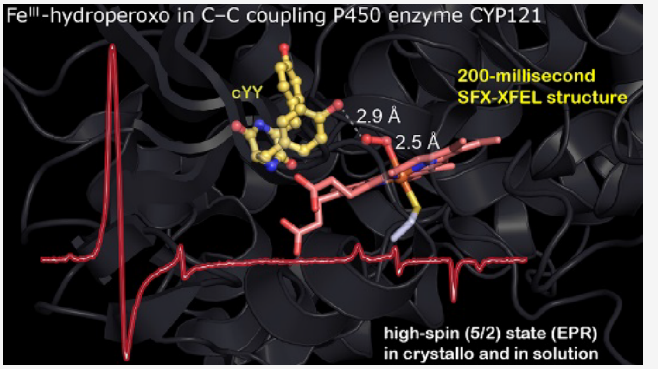

INTRODUCTION

The heme prosthetic group is ubiquitous, and its inimitable electronic properties are utilized by nearly every aerobic organism to catalyze a wide array of chemical reactions. Heme-based enzymes such as catalase, oxygenase, peroxidase, and peroxygenase share catalytic intermediates in the early stage of their reactions, which then deviate with distinct outcomes.[1] These intermediates can be short-lived, high-energy complexes, making their characterization a challenge. A ferric-bound hydroperoxo intermediate, often termed compound 0 (cpd 0), is a common reaction intermediate of diverse heme enzymes.[2] Cpd 0 is a precursor for the iron(IV)-oxo porphyrin π-radical cation intermediate, compound I (cpd I),[3] a popular active oxidant in heme-based chemistries (Scheme 1A). In some cases, the ferric-hydroperoxo intermediate can be used as an alternate oxidant to cpd I, such as in the proposed catalytic cycle of nitric oxide synthase and some engineered cytochrome P450 enzymes (CYPs).[4−6]

Cpd 0 is typically generated for characterization via cryoradiolytic reduction of the oxy-ferrous heme complex,[2,5,7−13] resulting in a ferric-peroxy anion intermediate, which is readily protonated to ferric-hydroperoxo by a proton delivery network in systems such as myoglobin, peroxidase, and catalase.[1] Due to its reactive nature and typical half-life of a

Received: May 15, 2023
Revised: September 27, 2023
Accepted: September 28, 2023
Published: November 8, 2023

https://doi.org/10.1021/jacs.3c04991
J. Am. Chem. Soc. 2023, 145, 25120−25133

Scheme 1. (A) Typical Catalytic Shunt Pathway in Cytochromes P450, including CYP121 with a Substrate Analogue, cYY(O)Me, and (B) Proposed Catalytic Pathway for CYP121 with Its Native Substrate[a]

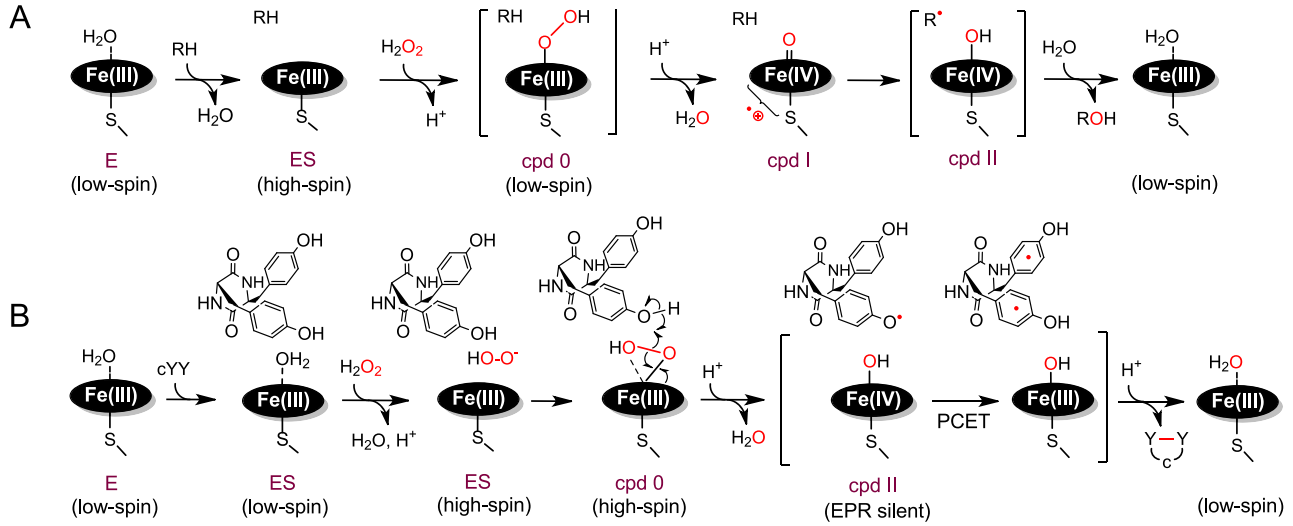

[a]The bracket represents the proposed intermediates, and PCET = proton-coupled electron transfer.

millisecond (ms) or less, structural characterization of cpd 0 has been elusive from intermediates trapped during catalysis. Only very recently has a cpd 0 crystal structure captured during catalysis been obtained in the histidine-ligated heme-based tyrosine hydroxylase with an alternate fluorinated substrate[14] and lactoperoxidase with iodide in the active site.[15] In the P450 catalytic cycle, the dioxygen of cpd 0 has been proposed to bind in an end-on mode,[4] which is supported by experimental and theoretical evidence.[5] All reported ferric-oxo/hydroperoxo intermediates in heme-based biological systems are thus far situated with the oxygen species ligated to the heme iron in the end-on orientation, resulting in a six-coordinate low-spin heme complex.

CYP121 is a cytochrome P450 enzyme from *Mycobacterium tuberculosis* that catalyzes the formation of mycocyclosin through a two-electron and O_2-dependent reaction via the intramolecular C−C coupling between the tyrosyl moieties of *cyclo*(L-tyrosine-L-tyrosine) (cYY).[16] This enzyme is essential for the viability of *M. tuberculosis*,[17] making it a potential drug target.[18] Its reaction has an unusual characteristic at the first step of the catalytic cycle,[19] where substrate binding does not trigger a full-spin transition of the heme from low- to high-spin, as is typically observed in most P450 enzymes (Scheme 1A). The low- to high-spin-state transition can be initiated with the binding of a synthetic probe, cYY(O)Me, where CYP121 shows its true color as a P450 hydroxylase.[20] The enzyme−substrate (ES) complex of CYP121−cYY remains primarily low-spin (Scheme 1B), with a minor portion of high-spin observed at g = 8.10, 3.50, and 1.70 (Figure 1A, trace I), indicating partial spin conversion. An X-band ENDOR study has shown that the lack of a clean spin transition is due to an equilibrium between distal ligand-free, hydroxide, and aqua ligands.[21] The reaction catalyzed by CYP121 can also produce mycocyclosin through a catalytic shunt using hydrogen peroxide or peracetic acid (PAA). This organic peroxide is known to contain a percentage of hydrogen peroxide in solution due to manufacturing methods.[22] Transient kinetic studies using stopped-flow UV−vis and rapid freeze-quench EPR (RFQ-EPR) to observe the reaction of CYP121 with cYY and PAA show no spectroscopic sign of cpd I accumulation in CYP121, but rather, an unusual high-spin intermediate is observed after PAA addition and prior to the product formation.[19] A nearly complete conversion of the ES complex to the high-spin ferric heme-based intermediate has previously been observed, which formed in solution in the dead time of mixing after the ES complex reacting with PAA.[19] The rapidly formed high-spin (S = 5/2) ferric intermediate was observed by RFQ-EPR with partial rhombicity and observed g-values of 6.87, 5.77, and 2.00 (Figure 1A, II).

The 5 ms high-spin intermediate observed by RFQ-EPR is the first of its kind and thus unprecedented in heme chemistry. It has been proposed to be a putative unusual cpd 0 intermediate.[19] The unique high-spin state of the intermediate is not the low-spin to high-spin transition induced by substrate binding observed in many P450 and other heme enzymes in the process of substrate binding for the formation of the ES complex (Scheme 1A).[20,23] Instead, this putative high-spin cpd 0 intermediate is generated by the oxidation of the ES complex. It is unprecedented as all cpd 0 intermediates described thus far are low spin. In the millisecond time domain, this high-spin ferric intermediate decays to an EPR-silent species. Until now, the chemical nature of the high-spin ferric heme-based intermediate remains uncharacterized.

In this work, EPR spectroscopy of a slurry of single crystals used was used to reproduce *in crystallo* the unusual 5 ms high-spin intermediate. In an effort to structurally characterize this *in crystallo* observed high-spin intermediate, we further developed and optimized the Drop-on-Tape single-crystal rapid-mixing method described elsewhere[24,25] and which enabled time-resolved serial femtosecond crystallography with X-ray free-electron laser (tr-SFX-XFEL) technology to directly access reaction intermediate crystal structures in the millisecond time domain at room temperature without freezing at any step of the structural determination. With this updated rapid-mixing method, we can observe directly and in real time the unusual high-spin ferric intermediate of the CYP121 reaction at room temperature without quenching. These efforts led to the structural illustration of the unusual intermediate and its rationale for the high-spin state. The results suggest an atypical P450 mechanism by which CYP121 utilizes cpd 0 and

https://doi.org/10.1021/jacs.3c04991
J. Am. Chem. Soc. 2023, 145, 25120−25133

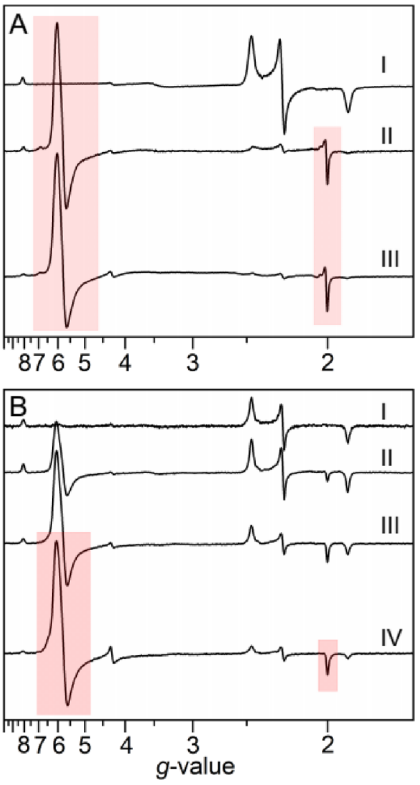

Figure 1. High-spin intermediate observed by rapid freeze-quench (RFQ) EPR of the solution state and single-crystal slurry EPR of the crystalline state after the reaction of the cYY−CYP121 complex with PAA. (A) RFQ-EPR of the solution state CYP121. The top spectrum represents the ES complex (I), the middle spectrum is from the ES complex after a 5 ms reaction with PAA (II), as reported previously,[19] and the bottom spectrum is the ES complex reaction with PAA after 500 ms of mixing time (III). The typical low- to high-spin transition is absent from the E to ES complex. After a 5 ms reaction, a new high-spin ferric heme is observed, which persists up to 500 ms before decay begins to occur. The signals pertaining to the rhombic high-spin species are highlighted with a red box. (B) Single-crystal EPR with a slurry of large-sized ES complex crystals. The top spectrum (ES, I) represents the crystals measured without PAA. Subsequent time points used parallel samples of the ES complex single-crystal slurry reacting with 5 mM PAA. The ES complex spectrum is magnified 2.5×, so the relative size of high-spin and low-spin signals is comparable to other spectra. Upon the reaction of the single-crystal slurry with PAA, an initial axial high-spin EPR signal can be observed by 30 s (II). A smaller rhombic high-spin EPR signal appears at 60 s (III) and then plateaus by 120 s (IV). The high-spin ferric heme intermediate observed both in RFQ-EPR and in *in crystallo* reaction EPR is highlighted with a colored box.

subsequently iron(IV)-oxo, compound II (cpd II), to oxidize its cYY substrate in a peroxidase-like outcome for C−C coupling.

EXPERIMENTAL PROCEDURES

Protein Expression and Purification. The methods for growth and expression of CYP121 from *M. tuberculosis* in *Escherichia coli* strain BL21(DE3) and purification have been previously described.[19−21] The isolated enzyme is known to be a functional homodimer with a buried surface area of 1300 Å^2 based on the recent ^{19}F NMR studies,[26−28] although it crystallizes as a monomer. The enzyme purity was judged based on SDS-PAGE electrophoresis and R_Z values, and the activity assay was described previously.[19,20] PAA was purchased from Sigma-Aldrich and contained 39% PAA and 6% hydrogen peroxide (13% of the total peroxide).

Preparation of Crystal Complexes. The *N*-terminal His_6-tag was cleaved off, and CYP121 was then cocrystallized with cYY using the procedure described previously.[20,21] Crystals were obtained from drops with a 1:1 ratio of the preformed ES complex (10−14 mg/mL enzyme in 50 mM Tris-HCl pH 7.4, 2 mM cYY) to mother liquor solution after a growth period of 2−4 weeks. Figure S1 shows the packing in the crystal lattice.

Stopped-Flow Absorption Spectroscopy. Stopped-flow studies were carried out on an Applied Photophysics SX20 stopped-flow system using a photodiode array to obtain multiwavelength kinetic data. The assay conditions consisted of 5 μM CYP121, 400 μM cYY, and 0.25−32 mM hydrogen peroxide after rapid mixing. A stock solution of 76 mM cYY was made by dissolving the substrate in DMSO, keeping the DMSO concentration at less than 2% (v/v) after mixing. To mitigate enzyme degradation from the addition of concentrated amounts of DMSO, the substrate was suspended in buffer before the addition of enzyme. Experiments were carried out at 22 °C in 100 mM potassium phosphate buffer at pH 5, 7.4, and 9.

Rapid Freeze-Quench EPR Spectroscopy. Experiments were carried out using a System 1000 chemical/freeze-quench apparatus made by Update Instruments, Inc. A liquid ethane or isopentane bath maintained at −155 °C was used to rapidly freeze the sample, as described previously.[19,29] Reactions were carried out by mixing 409 μM CYP121 and 1 mM cYY with 20 mM PAA in a 1:1 ratio at room temperature in a buffer consisting of 50 mM Tris-HCl, pH 7.4. The reaction mixture was rapidly frozen in liquid ethane after the reaction at varying time intervals in the millisecond time domain and carefully packed into EPR tubes. The excess liquid ethane was gently vacuumed off, and freeze-quenched samples were stored in liquid nitrogen until analysis. The EPR spectra were recorded at a 9.4 GHz microwave frequency with a 1.002 mW power using a Bruker E560 EPR spectrometer with an SHQE-W resonator at a 100 kHz modulation frequency and a 0.6 mT modulation amplitude. The temperature was maintained at 10 K by a cryogen-free 4 K temperature system for data collection. Studies using hydrogen peroxide as the oxidant were carried out with similar enzyme and substrate concentrations with an oxidant concentration of 32 mM and mixed in a 1:1 ratio.

Single-Crystal Slurry EPR Spectroscopy. Crystals of similar size (∼500 μm) and shape (needle-like) were collected in a 1.5 mL Eppendorf tube to a final crystal volume of ∼50 μL and a total mother liquor volume of 500 μL. The solution containing a crystal slurry was mixed homogeneously and 100 μL placed into a 4 mm quartz EPR tube containing mother liquor for a final volume of 200 μL. Crystals were evenly dispersed throughout the sample before rapidly freezing in liquid ethane to measure the ES complex. Parallel samples were made, and PAA was added to a final concentration of 5 mM, rapidly mixed with manual stirring, and frozen for each time point. Quantitative simulation of the EPR spectra was performed with EasySpin,[30] and the simulation parameters are given in Table S1.

Product Analysis. Crystals previously harvested and stored were used for the reaction with PAA. An aliquot of crystals was placed in a new 1.5 mL Eppendorf tube after the crystals were resuspended in the storage tube. The crystals were pelleted, and crystallization buffer was removed and set aside for use as control samples leaving approximately 10 μL of crystal volume. The control sample was partitioned into two tubes, with one charged with PAA to a final concentration of 2 mM. A fresh PAA solution (2 mM) was prepared in a crystallization buffer and used to resuspend the crystals. The reaction was stopped after 1 h by pelleting the crystals and removing the supernatant, which was then filtered with a 10 kDa centrifugal filter (Millipore) before 20 μL of filtrate was loaded onto an InertSustain C18 column (5 μm particle size, 4.6 × 100 mm, GL Sciences Inc.). The samples were analyzed using a Thermo Scientific Ultimate-3000SD HPLC rapid separation system equipped with a photodiode array detector. The chromatograms were recorded with a full range of wavelengths from 190 to 800 nm, and HPLC profiles presented in this study were chromatograms monitored at 295 nm. The elution method has been previously described.[19]

https://doi.org/10.1021/jacs.3c04991
J. Am. Chem. Soc. 2023, 145, 25120−25133

Structural Determination. The tr-SFX-XFEL diffraction data were collected at the Linac Coherent Light Source (LCLS), Menlo Park, CA, during experiments LU50, LV43, P112, and P199A. The ES complex crystals were vortexed using a Teflon bead (Hampton Research Inc.) to reduce their size to ∼30 μm in a 1.5 mL Eppendorf tube and the appropriate mother liquor. Vortexing caused the crystals to crack in in all three dimensions, greatly reducing their size and increasing their surface area. The resulting microcrystal slurry was measured for the resting state or mixed with PAA directly before X-ray exposure using the drop-on-drop approach described recently and updated in the main text. In this setup, the crystal slurry was dispensed onto a Kapton conveyor belt in the form of 2 nL droplets at a 30 Hz deposition frequency using an acoustic injector,[24] resulting in a sample consumption rate of 3.6 μL/min. A second droplet dispenser located 40 mm upstream of the X-ray interaction point was used to dispense a burst of 10 droplets of 60 pL each of a 250 mM stock solution of peracetic at a rate of 1.6 kHz onto the same conveyor belt.[25] Droplet ejection was triggered in such a way that two droplets out of each burst hit and were mixed with each of the larger crystal slurry drops, resulting in a final concentration of 14 mM PAA in the crystal-containing drop. The drops were transported at a belt speed of 200 mm/s from the droplet mixing point to the X-ray interaction point, resulting in a delay between mixing and X-ray probing of 200 ms. Diffraction data were collected at 1.30 Å wavelength using a Rayonix MX340-HS detector in a 4 × 4 binning mode at a repetition rate of 30 Hz with 4 mJ/pulse (LU50) or 2.2 mJ/pulse (LV43), a pulse duration of ∼35 fs, and an X-ray beam size at the sample of ∼3 μm in diameter.

Data acquisition was tracked with the cctbx.xfel graphical user interface.[31] The jobs run the core program dials.stills_process to index and integrate the images while providing real-time feedback, as part of the larger cctbx.xfel and DIALS processing suite.[32−36] A first estimate of the detector position (distance and beam center) was obtained from a powder diffraction pattern of silver(I) behenate (Alfa Aesar). After the initial spot finding, followed by indexing strong reflections and integration using dials.stills_process, a round of metrology refinement was done. The second round of indexing and integration was performed with the refined detector position. After correction of the integrated intensities for absorption by the Kapton conveyor belt, final data integration and merging were performed using cctbx.xfel.merge using the ev11 error model[35] with the synchrotron structure (5WP2.pdb) as a reference.

The structural data refinement was completed using Phenix version 1.20.1-4487.[37] The small molecules used for modeling (YTT, HEM, and PEO for cYY, heme, and hydroperoxo) were fetched from the PDB, and Phenix generated the ligand restraints. Justification of the resolution cutoff for the merged data was determined based on multiplicity in the highest resolution shell and on $CC_{1/2}$ (monotonic decrease). The small-molecule parameter files (HEM and PEO) were downloaded from the PDB and refined into the structure one at a time by using the default restraints generated in Phenix. Restraints for the YTT ligand were imported from Phenix version 1.21 and used for refinement. The R_{free} test sets for each data set utilized the default setting in phenix.refine (10%), and Phenix was allowed to optimize this during refinement. To determine the occupancy level of the hydrogen peroxide heme ligand, the oxygen atoms of the ligand were analyzed in a stepwise reduction fashion, from 0.90 to 0.30, and refined at each step with the occupancies box unchecked in the refinement strategy. When the dictated occupancy level showed no overfitting or underfitting of the ligand model, the occupancies box was checked under the refinement strategy to allow Phenix to optimize the occupancy level of the ligand. The *B*-factors were held constant throughout the refinement tests.

RESULTS

Observation of the High-Spin Intermediate by Single-Crystal Slurry EPR Spectroscopy. The production phase of the high-spin ferric heme-based intermediate after peroxide addition to the ES complex is before the dead time of the freeze-quench setup in the solution state by RFQ-EPR. Here, we attempted to observe this intermediate in the crystalline state. The single crystals of CYP121 in complex with its substrate, cYY, were obtained, as described previously.[20,21] For EPR measurement of the ES complex, approximately 1000 equivalent cocrystallized single crystals in a mother liquor solution were transferred in random orientation to an EPR tube, flash-cooled with liquid ethane, and stored in liquid nitrogen. The large number of crystals used was necessary for signal averaging due to varying crystal orientations in the sample tube. EPR analysis of the crystal slurry revealed an expected six-coordinate, low-spin (LS) ferric heme species (g_z, g_y, g_x: 2.45, 2.24, 1.91), which matches the observed spectrum of the solution-state ES complex (Figure 1B, I). A small percentage of rhombic heme species was presented in the high-spin (HS) state with resonances observed at $g_{z,y}$ = 8.09, 3.55, and a g_x value indiscernible from the baseline is present. It belongs to the ES complex, not the resting state, as found previously.[19] Thus, the typical substrate-induced low- to high-spin transition for P450 enzymes is not observed in the EPR with a slurry of crystals, consistent with the solution EPR results. The majority of the cYY−CYP121 complex remains in the LS state.

Four parallel samples, each containing thousands of the ES complex crystals, were used for reaction with 5 mM PAA and flash-cooled in liquid ethane at progressive time points in each set of replicate experiments. The milliseconds time domain is inaccessible for EPR characterization of the *in crystallo* reaction using hand mixing, with the fastest access time being approximately 5 s for mixing, reaction, and freezing. Within 30 s of reaction, a new high-spin signal with observed *g*-values of 6.43, 5.76, and 2.00 appears in the spectrum (Figure 1B, II), which maximizes at 120 s (Figure 1B, IV). Formation of this signal is accompanied by near-complete disappearance of the initial ES complex high- and low-spin heme signal. Comparison of the single-crystal slurry EPR spectra to solution-state RFQ-EPR shows that the 60 and 120 s spectra are consistent with the 5−500 ms RFQ-EPR spectra shown in Figure 1A spectra II and III and Figure S2. Simulation of the 120 s spectrum without a rhombic six-coordinate high-spin component led to residuals showing imperfect fitting, indicating that the g = 6.43 resonance is an integral component of the spectrum (Figure S3). The minor *g*-value shift is due to the difference between the solution and crystalline states, as the g = 8.09 resonance of the ES complex was previously noticed at g = 8.11 in the solution state.[19] The relative concentrations of the EPR-active species and simulation parameters used for quantification can be found in Table S1, and each component used to reconstruct the entire 120 s single-crystal slurry EPR spectrum is listed in Figure S4. The simulation shows five components: a low-spin, five-coordinate high-spin, axial six-coordinate high-spin, rhombic six-coordinate high-spin, and isotropic g = 4.27 signal present in the spectrum.

Parallel-mode EPR detected no integer-spin signals from PAA oxidation of the crystal slurry. With the high concentration of PAA to maximize production of the 120 s high-spin intermediate, no regeneration of the initial low-spin species was noted during the decay of the intermediate high-spin signal. The similarity between the 120 s high-spin heme signal generated *in crystallo* and RFQ in solution supports the same intermediate formed in both states. To confirm that the high-spin species detected by EPR are on-pathway and therefore catalytically relevant, one intact crystal was exposed

https://doi.org/10.1021/jacs.3c04991
J. Am. Chem. Soc. 2023, 145, 25120−25133

to the oxidant and monitored by UV−vis spectroscopy on the minutes time scale. It was observed to transition from the cYY−CYP121 complex to the ligand-free CYP121 via the α/β and charge transfer bands, indicative of the product leaving the active site (Figure 2A). This was confirmed by a bulk *in*

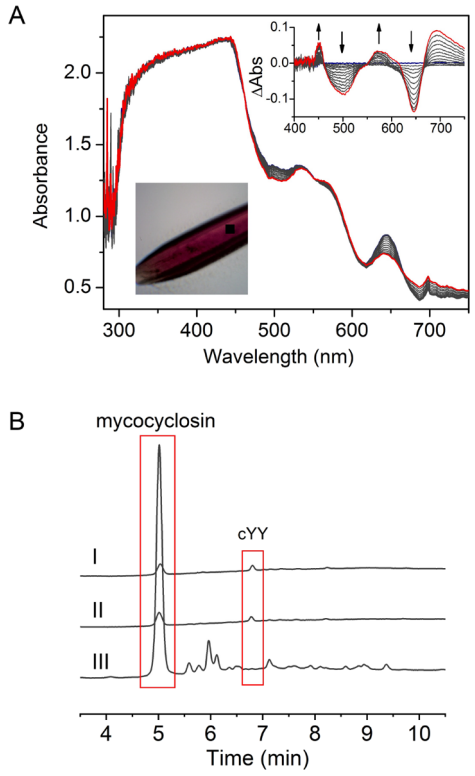

Figure 2. Single-crystal UV−vis monitoring of the CYP121 ES complex crystal reaction with PAA and the crystal reaction product analysis. (A) ES complex reaction with PAA monitored by a single-crystal UV−vis microspectrophotometer in real time. An image of the crystal and the difference spectra is shown in the inset, showing the initial ES complex spectrum (navy) transition to the E only state (red) concomitant with the shifting of the α/β band and decay of the charge transfer band. This ES-to-E transition is observed in the minutes time window depending on the size of the single crystal, and it suggests a substrate-to-product conversion. (B) HPLC analysis of the supernatant from the CYP121−cYY crystal reaction with PAA. (I) Mother liquor in which crystals are stored in, (II) mother liquor with 2 mM PAA, and (III) reaction of ES complex crystals with PAA after 60 min. The product, mycocyclosin, and substrate, cYY, elutions are highlighted with red boxes.

crystallo reaction where the supernatant analyzed by HPLC showed an elution at 5 min with the UV−vis spectrum correlating with previous reports of mycocyclosin (Figure 2B). Detection of mycocyclosin in conjunction with *in crystallo* reactions monitored by EPR resembled the solution-state reaction RFQ-EPR spectra, which indicates that these observed intermediates are indeed on-pathway and therefore mechanistically relevant.

Structural Characterization of the Early Intermediate by tr-SFX-XFEL. To access early reaction intermediates during CYP121 turnover, we improved our recently developed drop-on-drop method for studying reactions *in crystallo*.[24,25] This approach utilizes the Drop-on-Tape approach but includes a second droplet dispenser that allows for the addition of tiny volume droplets to a large crystal slurry containing drops at variable delay times before X-ray probing. A photograph of this mixing device is shown in Figure S5. This on-demand strategy rapidly mixes and initiates reactions of almost any substrate over a wide range of concentrations within any microcrystal slurry to study catalytic reactions ranging from tens of milliseconds to several seconds (see the Methods for details). Substrate concentration, mixing, and reaction initiation are a function of how many ∼30−80 pL volume droplets (between 0 and 50) are added with turbulent force to the approximately 2−4 nL crystal slurry drop as it moves toward the X-ray interaction region. Each particular reaction time point is determined by the speed of the Kapton belt and the distance between the droplet mixing point and the X-ray interaction region.[25] Compared to the previous version of the setup, we reduced the distance between the mixing point and the X-ray interaction region, enabling us to access shorter mixing times, and improved the control and visualization of the droplet collision region, allowing for the reproducible addition of a larger number of droplets to the microcrystal slurry drops. Since the tr-SFX-XFEL method requires microcrystals, we generated needle-like microcrystal slurries of the cocrystallized CYP121 ES complex, and each microcrystal within the slurry was approximately 30 μm in length or smaller. The unique high-spin intermediate formed in less than 5 ms in solution and within seconds in large crystals is expected to develop in the milliseconds time domain because the smaller size the crystal, the faster the ligand diffusion, and hence, the reactions.[14,38−40] The PAA used in the experiments is not a pure solution due to manufacturing methods and thus consists of approximately 39% PAA, 6% H_2O_2, and 55% acetic acid. We quantified the percentage of H_2O_2 present in the PAA solution used in our experiments to be 5.5 ± 0.3 wt % by ceric sulfate titration using previously reported methods.[22]

The tr-SFX-XFEL data set of the ES complex (Figure 3A) was refined to a 1.65 Å resolution (Table 1, PDB entry: 8TDQ). The tr-SFX data sets were obtained from an ES microcrystal slurry in mother liquor to which we added 14 mM PAA (optimized for the tr-SFX-XFEL setup), which contains 1.8 mM H_2O_2. Reaction times ranged from milliseconds to seconds at room temperature before reaching the X-ray interaction region for diffraction. The 200 ms tr-SFX-XFEL crystal structure of the intermediate was solved by molecular replacement and refined to a 1.85 Å resolution (Table 1, PDB entry: 8TDP). The atomic models for the 200 ms intermediate structure and the ES complex are very similar, with no significant identifiable electron density differences observed on the protein or the cYY substrate, but with apparent differences visible at the heme iron. Comparing the axial ligand electron density shape and ligand fittings of all tr-SFX data sets in hand from 200 ms to 90 s (the latter obtained by in-well mixing rather than the drop-on-drop strategy), we found that the 200 ms tr-SFX-XFEL electron density is fit most appropriately with an atomic model of a heme-bound hydroperoxo intermediate (cpd 0). This newly observed elongated electron density (Figure 3B) is not present in the ES complex or at longer reaction times at room temperature as determined by tr-SFX.

Assignment of the partial hydroperoxo axial ligand stems from observations of the RFQ-EPR spin-state transition from the 5 ms time point. An initial refinement of a water molecule into the ligand density of the 200 ms tr-SFX-XFEL data set resulted in an incomplete fit with excess electron density observed adjacent to the water and appropriately sized for an oxygen atom (Figure S6, panel B). Attempts to fit PAA into the

https://doi.org/10.1021/jacs.3c04991
J. Am. Chem. Soc. 2023, 145, 25120−25133

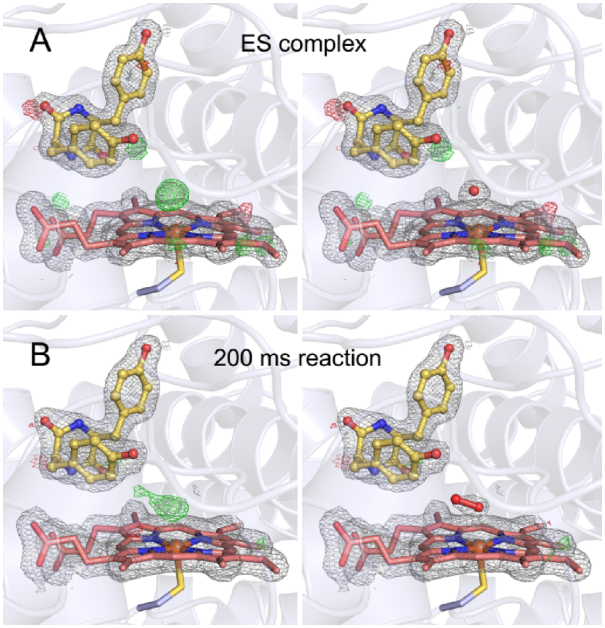

Figure 3. Hydroperoxyl ligand observed in situ by time-resolved SFX-XFEL of CYP121 cocrystallized with a cYY microcrystal slurry reacted with PAA for 200 ms. (A) ES complex at a 1.65 Å resolution (8TDQ.pdb) and (B) 200 ms intermediate at a 1.85 Å resolution (8TDP.pdb). The $2F_0-F_c$ electron density map is contoured at 1 σ (gray), and the F_0-F_c electron density map is contoured at 3 and −3 σ (green and red, respectively). The left panels show the omit map of the ES complex and the 200 ms intermediate without modeling the sixth ligand in the axial position of the heme iron. In contrast, the right panels show the electron density after modeling a ligand. For the 200 ms intermediate, the shape of the omit map is elongated rather than spherical, as expected for a water molecule. A peroxide ligand refined into the axial ligand density at 50% occupancy results in a consummate fitting, which shows the ligand residing in a near-side-on orientation relative to the heme iron.

axial ligand electron density at 100 and 50% occupancy resulted in unsatisfactory refinements (Figure S6C,D). At full occupancy, the peroxide ligand is clearly overfitted (Figure S7), whereas reducing occupancy to 50% yielded a satisfactory fit for all axial ligand electron density with no over- or underfitted difference features present (Figure 3B).

Notably, this peroxide ligand is relatively weakly associated with the iron ion. The Fe−O_1 and Fe−O_2 distances are 2.54 ± 0.11 and 3.22 ± 0.19 Å, respectively; the O_1-O_2 bond length is 1.42 ± 0.10 Å, and the Fe−S(Cys345) bond length is 2.27 ± 0.03 Å (Figure S8). The accuracy of these positional assignments was determined by perturbation of the structure factors ($\pm[F_{obs}-F_{model}]$) of the model using the END RAPID method, which allows the assignment of coordinate errors to individual atoms.[41] The structure factors are randomly perturbed in the target model generating 100 trials, followed by rerefinement of each of the perturbed data sets using Phenix, which generates standard deviations of the reported atom positions.

The observed Fe−O_1 and Fe−O_2 distances are greater than an expected Fe−O bond (average 2.15 Å length), indicating a weakly associated hydroperoxyl ligand in a five- or six-coordinate ferric heme center with a weak axial ligand, consistent with the high-spin state observed by EPR spectroscopy. An Fe−O_1-O_2 angle of 105.3° and a (Cys_{345})S−Fe−O_1-O_2 torsion angle of −171.87° further indicate that the peroxide ligand is situated in a near-side-on orientation. Thus far, nearside-on binding has not been observed in any heme-based biological systems and was previously only characterized in several model complexes.[42−48] It should be noted that this ferric-hydroperoxo structure differs from those reported in porphyrin model complexes with a mixed N/O ligand set. To date, neither end-on nor side-on peroxo intermediates have been structurally observed in heme-dependent iron enzymes with an axial thiolate ligand through direct observation or a trapping method. This ferric-hydroperoxo found in CYP121 with its native substrate is thus the first of its kind in thiol-ligated heme-based enzymes.

Table 1. Time-Resolved Room-Temperature SFX-XFEL Data Collection and Refinement Statistics for the ES Complex and 200 ms Reaction Intermediate with PAA

description	CYP121 + cYY (ES) no oxidant	cpd 0 intermediate Δt = 200 ms
PDB entry	8TDQ	8TDP
data collection		
no. of lattices used for refinement	10856	11569
space group	$P6_522$	$P6_522$
a, *b*, *c* (Å); *α*, *β*, *γ* (deg)	78.6, 78.6, 265.3; 90, 90, 120	78.7, 78.7, 265.9; 90, 90, 120
resolution	31.8−1.65 (1.68−1.65)[a]	33.2−1.85 (1.92−1.85)[a]
no. of unique reflections	58932	41826
redundancy	67.1 (9.8)	48.3 (8.1)
R_{split}[b]	0.14 (1.042)	0.20 (0.92)
$I/\sigma I$	4.54 (0.538)	3.01 (0.587)
completeness (%)	99.9 (99.7)	99.9 (98.9)
$CC_{1/2}$	0.984 (0.140)	0.84 (0.257)
refinement		
resolution (Å)	31.8−1.65 (1.71−1.65)	33.2−1.85 (1.92−1.85)
no. of reflections	59182	42609
R_{work}[c]/R_{free}[d] (%)	17.1/20.1	18.1/22.8
no. of atoms/*B*-factors (Å²)		
protein	3071/22.9	3065/31.6
heme	43/16.7	43/24.6
hydroperoxo	n/a	2/24.6
substrate[e]	24/24.1	24/31.3
solvent	325/33.1	285/39.0
bond lengths (Å)	0.007	0.008
bond angles (deg)	0.92	1.04
Ramachandran analysis		
favored (%)	99.2	99.0
allowed (%)	0.76	1.02
outliers (%)	0.00	0.00

[a]Numbers in parentheses refer to the data in the highest-resolution shell. [b]R_{aplit} was calculated by randomly splitting the available images into two halves, integrating both to prepare two half data sets, calculating the R-factor between them, and correcting for the reduction in multiplicity. [c]$R_{work} = \Sigma||F_0|-k|F_c||/\Sigma|F_0|$. [d]$R_{free}$ is the same as R_{obs} for a selected subset (10%) of the reflections that were not included in prior refinement calculations. [e]The substrate involved is *cyclo*(L-Tyr-L-Tyr).

Rapid Freeze-Quench EPR Probes the Protonation State of the Observed Structural Intermediate from SFX. While the tr-SFX-XFELS structure study shows an unprecedented axial hydroperoxo heme ligand, an observed Fe−O_1 bond length of 2.54 Å is significantly longer compared

https://doi.org/10.1021/jacs.3c04991
J. Am. Chem. Soc. 2023, 145, 25120−25133

Table 2. Fe−O Bond Distances in Structurally Characterized Enzyme and Model Ferric-Peroxo/Hydroperoxo Complexes

enzyme	intermediate	Fe−O (Å)	O−O (Å)	methodology	PDB entry	ref
CYP121 (ternary)	ferric-hydroperoxo	2.5	1.4	direct observation	8TDP	this work
CYP121 (binary)	ferrous-oxy	2.14	1.23	synchrotron radiation	1N40	49
tyrosine hydroxylase (TyrH)	ferric-hydroperoxo	2.2, 2.4	1.4, 1.4	directly trapped	7KQU	14
lactoperoxidase	ferric-hydroperoxo	2.41, 2.33	1.48, 1.49	directly trapped	7DN6, 7DN7	15
chloroperoxidase	ferric-hydroperoxo	1.8	1.5	photoreduction	2J5M	2
myoglobin (sperm whale)	ferric-peroxo	1.85	1.33	synchrotron radiation	2Z6T	10
myoglobin (horse heart)	ferric-peroxo, ferric-hydroperoxo	1.84, 1.78	1.34, 1.50	cryoreduction	2VLX	11
oxy-F33Y-CuB-myglobin (sperm whale)	ferric-hydroperoxo	1.84	1.22	cryoreduction	5HAV	12
H128N catalase	ferric hydrogen peroxide complex	2.56, 2.89, 3.01, 3.29	1.54, 1.51, 1.52, 1.52	mutation, soaking	1GGF	50

model complex	compound	Fe−O (Å)	O−O (Å)	methodology	ref
$[Fe^{III}([15]aneN_4)(SC_6H_5)(OO^tBu)]^+$	ferric-alkylperoxo	2.74	3.03	synthesized	51
$[Fe^{III}([15]aneN_4)(SC_6H_4\text{-}p\text{-}Cl)(OO^tBu)]^+$	ferric-alkylperoxo	2.75	3.03	synthesized	51
$[Fe^{III}([15]aneN_4)(SC_6H_4\text{-}p\text{-}OMe)(OO^tBu)]^+$	ferric-alkylperoxo	2.71	3.03	synthesized	51
$[Fe^{III}([15]aneN_4)(SC_6H_4\text{-}p\text{-}NO_2)(OO^tBu)]^+$	ferric-alkylperoxo	2.77	3.02	synthesized	51
$[Fe^{III}([15]aneN_4)(SC_6H_4\text{-}p\text{-}SC_6F_5)(OO^tBu)]^+$	ferric-alkylperoxo	2.85	3.01	synthesized	51

to an average of 1.8 Å for a heme-based oxygen ligand reported in other low-spin heme peroxo structures but only slightly longer than the 2.3 Å average length observed for cpd 0 directly trapped in the reaction with a substrate in histidyl-ligated heme-based enzymes (Table 2).[14,15] Reported Fe−O bond distances for nonporphyrin-based model complexes with a thiolate-aryl ligation and *tert*-butyl-peroxide ligand are longer, ranging from 2.74 to 2.85 Å. Additionally, the observation of a hydroperoxo rather than a peracetate ligand when an organic alkyl peracid is used raises questions.

As mentioned, the PAA solution consists of acetic acid, PAA, and H_2O_2 with corresponding pK_a values of 4.8, 8.2, and 11.8, respectively. Due to the multiple components present in solution, we interrogated the effect of each component on the formation of the heme axial ligand and defined that the high-spin species is generated specifically by PAA and not H_2O_2 or acetic acid. Additionally, the effect of pH on cpd 0 formation using hydrogen peroxide was screened to ensure that the lack of observed high-spin species was not due to the protonation state. First, with the high amount of acetic acid present in the oxidant solution, the effect of pH on the formation of the high-spin signal was screened using hydrogen peroxide as the oxidant to determine its ability to initiate the low- to high-spin transition. A pH range of 5−9 was screened by RFQ of the ES complex reacting with hydrogen peroxide and measured by EPR to determine whether a high-spin signal similar to that observed when using PAA would be generated (Figure S9). When monitoring the reaction within this pH range at progressive time points, the dominant species remained low-spin heme with a small fraction of high-spin heme present, indicating that hydrogen peroxide does not contribute to the high-spin heme intermediate despite the observation of the hydroperoxo ligand in the tr-SFX-XFEL structure. Additionally, at high pH and long reaction time points, a minor equilibrium low-spin species is observed with *g*-values of 2.32 and 2.17 (Figure S10). These *g*-values correspond to those ferric-hydroperoxo heme species from cytochrome P450 that have been artificially generated by cryoradiolytic reduction and characterized.

Next, a 10% H_2O_2 solution was made using glacial acetic acid to mimic the conditions of the PAA solution, no PAA, and aged for a minimum of 24 h at 4 °C. The buffer capacity was increased to 250 mM to ensure that the pH was maintained constant upon mixing oxidant with the ES complex. At early time points, no low- to high-spin transition is observed. In the seconds time domain, a small fraction of low-spin heme transitioned to the high-spin heme species (Figure 4A). This signal was normalized to the high-spin intermediate generated via PAA in 5 ms and overlapped well, indicating that the same cpd 0 intermediate is formed in both cases (Figure 4B). The use of acetic acid alone did not generate the high-spin signal at any time point (Figure S11), demonstrating that only the hydrogen peroxide in acetic acid is able to form the cpd 0 intermediate, albeit less efficiently compared to PAA.

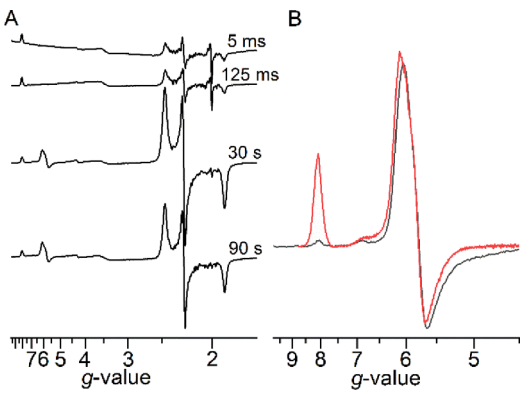

Figure 4. A small fraction of the high-spin cpd 0 intermediate is generated from H_2O_2 in glacial acetic acid. (A) CYP121 ES complex rapidly mixed with the oxidant for 5 and 125 ms and hand-mixed for 30 and 90 s. In the millisecond time points, the heme remains low-spin with a small observable radical signal. In the seconds time points, a small fraction of the high-spin intermediate different from that generated by substrate binding is observed. (B) Overlay of the RFQ-EPR 5 ms high-spin ferric heme-based intermediate observed when using H_2O_2 in PAA (red) and glacial acetic acid (black) as the oxidant.

https://doi.org/10.1021/jacs.3c04991
J. Am. Chem. Soc. 2023, 145, 25120−25133

Table 3. Comparison of the *g*-Values of Hydroperoxo Heme Species in Cytochromes P450 and Other Heme-Dependent Enzymes

enzyme	method	substrate	high-spin g_1, g_2, g_3	low-spin g_1, g_2, g_3	hydroperoxo g_1, g_2, g_3	ref	chemistry
CYP121		none	8.10, 3.50, 1.7	2.49, 2.25, 1.89		19	C−C bond forming
CYP121		cYY[a]	8.11, 3.50, 1.7	2.45, 2.25, 1.90		19	
CYP121	oxidant	cYY+PAA[b]	8.09, 3.50, n.d.	2.45, 2.25, 1.90	6.87, 5.77, 2.00	19, this work	
CYP121	oxidant	cYY+H_2O_2	8.10, 3.50, n.d.	2.48, 2.25, 1.90	2.32, 2.17, n.d.	this work	
P450cam	cryoradiolytic reduction	camphor	8.0, 4.0, 1.8	2.41, 2.21, 1.96	2.29, 2.17, 1.96	53,56	O atom insertion
P4502B4	O_2-saturated buffer	Bnz[c]+CPR[d]	8.11, 3.55, n.d.	2.41, 2.23, 1.92	2.32, 2.16, 1.95	54,57	O atom insertion
P450ssc	cryoradiolytic reduction	none			2.34, 2.18, 1.95, 2.37, 2.18, 1.95	55,58	O atom insertion
horseradish peroxidase	cryoradiolytic reduction	none			2.32, 2.18, 1.94	59	reduction
chloroperoxidase	cryoradiolytic reduction	none			2.28, 2.18, 1.95	59	halogenation

[a]cYY, *cyclo*(L-tyrosine-L-tyrosine). [b]PAA, peracetic acid. [c]Bnz, benzphetamine. [d]CPR, cytochrome P450 reductase (n.d., not determined).

It is important to distinguish between two possibilities for the chemical nature of the high-spin intermediate observed in the *in crystallo* reactions, RFQ-EPR solution-state studies, and tr-SFX-XFEL structure induced with PAA: (1) a very weakly associated, singly protonated peroxo ligand or (2) a fully protonated hydrogen peroxide adduct. As noted before, H_2O_2 is not as catalytically efficient as PAA in the CYP121−cYY reaction at pH 7.4 and 9, and a higher H_2O_2 concentration is needed for substrate turnover.[19,20] Next, we revisited the pH dependence of the PAA-dependent reaction. Stopped-flow absorption spectroscopy was used to track the enzymatic reaction with hydrogen peroxide at pH 5, 7.4, and 9, which distinctly differs from the reaction kinetics of PAA (Figure S12). As previously characterized, upon addition of PAA, a transition from the ES complex to E is observed, with the decrease of the 395 nm band and concomitant increase at 427 nm within 300 ms, which redshifts over time to 433 nm.[19] The use of H_2O_2 resulted in stark differences from PAA where an initial decrease of the ES complex Soret band at 395 nm and an increase at 419 nm within 50 ms were observed with no obvious changes elsewhere on the spectrum (Figure S13). At 100 ms, this 419 nm band disappears, and the major shift turns to the decrease of the ES complex Soret up to 5 s with a band increasing at 441 nm through 60 s of the reaction. As the pH increases, the initial transition observed within 50 ms is much less pronounced. Over a period of 60 s, the enzyme-only Soret band expected at 419 nm never recovers, likely due to an equilibrium species from the high concentration of hydrogen peroxide used. The RFQ and hand-mixed EPR samples of the ES complex reaction with H_2O_2 at pH 5 used to probe the heme center at progressive time points revealed a similar observation regarding spectral differences compared to PAA (Figure S9A). As described above, no low- to high-spin transition of the heme is observed when H_2O_2 is used alone as the oxidant. Rather, the initial transition within 30 ms results in a decrease of low-spin signal intensity coupled with the appearance of a minor radical signal at g = 2.008, which maximizes between 125 and 500 ms and then disappears in the seconds time domain. The decrease of the low-spin signal indicates the formation of an EPR-silent species, likely cpd II, and the signal is not fully reformed until after 500 ms. The small percentage of high-spin signal observed in both the E and ES complexes does not change throughout the reaction, indicating that it is an inactive form of the heme. These details are in stark contrast to the use of PAA as an oxidant where upon mixing with the ES complex, a rhombic high-spin heme species in the *in crystallo* reactions is detected. Thus, with the use of H_2O_2 and lack of formation of the PAA-induced high-spin ferric heme-based intermediate previously observed, the 200 ms structure represents a cpd 0 intermediate corresponding to the unique six-coordinate rhombic high-spin heme observed in solution-state RFQ and single-crystal slurry EPR.

DISCUSSION

The cpd 0 heme intermediate in cytochromes P450 has been extremely challenging to directly capture due to its inability to accumulate before cpd I formation. Thus, the major technique that has been deployed to generate this intermediate is the cryoradiolytic reduction of the oxy-ferrous P450 complex at low temperatures coupled with an annealing process at progressively higher temperatures to track the degradation of the ferric-hydroperoxo complex.[52] These trapped and characterized complexes of oxygen-inserting enzymes, P450cam,[53] P4502B4,[54] and P450ssc,[55] have the ferric-hydroperoxo as low-spin heme, consistent with a six-coordinate end-on hydroperoxo ligand (*g*-values summarized in Table 3). In sharp contrast, the observations described in this study indicate the presence of a high-spin (S = 5/2) cpd 0 intermediate (Scheme 1B), observed in solution and *in crystallo* initiated by adding an oxidant and observed at room temperature.

Those reported ferric-hydroperoxo intermediates generated by cryoradiolytic reduction are representative of hydroxylating P450s but do not necessarily include the less studied subset of P450s that perform other chemistries such as C−C and C−N bond-forming/bond-breaking reactions. Initiating the CYP121 C−C coupling reaction with PAA yields a high-spin heme signal that has never been reported in thiolate-ligated heme systems and, to the best of our knowledge, is unique to the CYP121 ternary complex. Indeed, if a high concentration of H_2O_2 is mixed with enzyme and reacted for 40 s, a minor ferric-hydroperoxo heme (g = 2.32, 2.17, n.d.) is observed that is consistent with those cryoradiolytically reduced cpd 0

https://doi.org/10.1021/jacs.3c04991
J. Am. Chem. Soc. 2023, 145, 25120−25133

intermediates. However, due to the long time point, this is likely an inactive equilibrium heme species rather than an on-pathway intermediate.

The approximately 600-fold increase in the reaction rate observed in the microcrystals used for the tr-SFX-XFEL experiment compared with large crystals used for EPR spectroscopy is a significant rate change. The microcrystals were prepared by vortexing large crystals, which were shattered in all three dimensions. While this reduces the crystal size and thickness, the exposed surface area is greatly increased, which means that the oxidant can diffuse through a small crystal more easily than a large crystal. Additionally, the crystal packing for CYP121 is quite tight, which slows the diffusion rate. This effect is clearly visible also in single-crystal absorption spectroscopy measurements, where the transition of the ES complex to E upon addition of oxidant is dependent upon the crystal size, where larger, thicker crystals take longer (~15 min) to begin the transition compared to smaller, thinner crystals (~6 min). An image of the crystal size difference between microcrystals and large crystals is shown in Figure S14.

Modeling of an H_2O_2 ligand into the 200 ms tr-SFX-XFEL structure led to questions regarding the O atom source, considering that the oxidant used for the reaction is PAA, which is not observed in the active site. Because PAA is not a pure solution, the other components were screened for their potential role in the formation of the intermediate and to determine whether PAA or hydrogen peroxide is the active oxidizer. The peroxides reside in an acidic solution and are mostly protonated. Thus, the impact of pH on the ability of hydrogen peroxide to form the high-spin species was screened from pH 5 to 9 to test the capability of this small molecule to ligate to the heme iron in different protonation ratios. The lack of high-spin species generated at both low and high pH indicates that hydrogen peroxide is not able to easily ligate to the heme iron and initiates catalysis, regardless of its protonation state, which is corroborated by the lower level of product generation compared to PAA. Because PAA is generated in an equilibrium reaction by mixing hydrogen peroxide and glacial acetic acid,[60] a 10% hydrogen peroxide oxidant solution was made using this method and stored for a minimum of 24 h at 4 °C. In this instance, a small amount of PAA is expected to be generated, which would form the high-spin heme species. Indeed, this occurs, although at a long time point, likely due to the low concentration of PAA present in solution. At pH 7.4, fewer than half of the PAA molecules are deprotonated. However, it is likely that these deprotonated molecules ligate to the heme iron more readily and lead to higher levels of product formation, which is observed during activity assays when the pH is increased.[20]

It has been demonstrated through computational and model complex studies that the spin state of the ferric-hydroperoxo complex is vital for its reactivity.[61,62] The high-spin state of a ferric hydrogen peroxide adduct due to the weak association and near-side-on geometry of the hydrogen peroxide moiety with the iron ion is a novel observation. Comparison of the 2.27 Å heme Fe−S bond length of the 200 ms intermediate to other reported synchrotron X-ray and SFX structures (Table S2) shows that this high-spin state is solely due to the weak association of the near η^2-hydrogen peroxide adduct, and a comparable iron−sulfur bond distance at 2.37 Å on the proximal side of the heme as found in the ES complex structure. An early EPR study comparing the high-spin EPR signal of P450s to thiolate-ligated iron porphyrin complexes determined that the presence of the thiolate ligand to the iron ion increased the rhombicity of the high-spin signal compared to complexes with an oxygen or nitrogen axial ligand due to the thiolate pushing the metal ion out of the plane of the porphyrin ring.[63] Nearly a decade later, another study reported an *N*-ligated peroxo-porphyrin complex with a peroxo ligand presenting a rhombic, high-spin species by EPR, although its orientation to the iron ion could not be fully resolved.[42] In this instance, the high-spin ferric signal is rhombic, with *g*-values of 9.50, 4.20, and 1.30. More recent studies of *N*-ligated porphyrin complexes characterized both the side-on and end-on peroxo/hydroperoxo orientations via spectroscopic methods.[46,47] The decay of the side-on to end-on peroxo orientation is observed by protonation of an oxygen atom, tracked by the decay of the g = 4.20 EPR signal to the rhombic low-spin porphyrin complex, corresponding to an end-on ferric-hydroperoxo complex. Thiolate-ligated model complexes used to study the nonheme enzyme superoxide reductase are able to generate a mononuclear ferric-alkylperoxo or hydroperoxo complex upon addition of the corresponding alkylperoxide or O_2, with the complexes reported as low-spin by EPR, likely arising from a six-coordinate end-on species.[51,64,65] These model complexes give great insight into the spectroscopic characteristics of an unusual side-on ferric-hydroperoxo intermediate structurally observed for the first time in a thiolate heme-based biological system, which determines that the high-spin signal captured in RFQ and single-crystal slurry EPR studies is indeed a weakly associated hydrogen peroxide cpd 0 intermediate. Additional stopped-flow and RFQ-EPR experiments at low pH using hydrogen peroxide resulted in the intensity of the low-spin signal decreasing, potentially due to an accumulating cpd II species and no low- to high-spin transition. After a brief period of time, the low-spin signal reforms.

Comparing this high-spin, ferric-hydroperoxo intermediate with previously reported ferric-peroxo intermediate structures reveals a stark difference in the hydroperoxo binding orientation relative to the heme iron. Those published crystal structures of a ferric-hydroperoxo intermediate directly trapped in an enzyme-mediated catalytic cycle are from histidine-ligated heme-based tyrosine hydroxylase[14] (TyrH) and lactoperoxidase[15] (Figure 5), with all other structures such as chloroperoxidase[2] and myoglobin[10,11] obtained from radiolytic methods (Figure S15). A CYP121 crystal structure bound with O_2 in an end-on orientation was also previously reported, which was crystallized in the ferric state and observed due to the synchrotron X-ray beam reduction of the iron center.[49] Comparison of the CYP121 ES complex, enzyme-O_2 bound, and cpd 0 intermediate structures is described in Figure S16.

The bond distance range and coordination angles reported for those previously characterized ferric-peroxo intermediates of Fe−O (1.9−2.5 Å), O−O (1.3−1.6 Å), and Fe−O−O (119−138°) are different from the values observed in the CYP121 ferric-hydroperoxo intermediate, which has an Fe−O_1 bond length of 2.5 Å, an Fe−O_2 interaction of 3.2 Å, an O−O bond length of 1.4 Å, and an Fe−O−O coordination angle of 105.3° (Table S2). The coordination angle of this intermediate falls well outside the range for reported end-on peroxo intermediates from myoglobin,[10,11] peroxidase,[2] TyrH,[38] and lactoperoxidase.[15] It sets the chemistry apart from other reported P450 enzymes. Heme distortion may also be a contributing factor in the more side-on binding orientation of

https://doi.org/10.1021/jacs.3c04991
J. Am. Chem. Soc. 2023, 145, 25120−25133

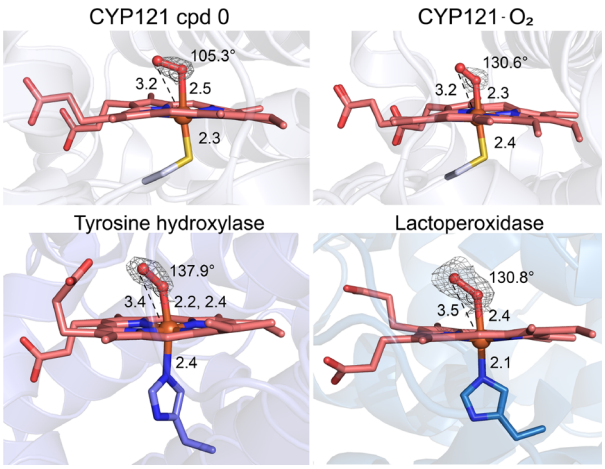

Figure 5. Structural comparison of the observed time-resolved SFX-XFEL ferric-hydroperoxo intermediate of P450 CYP121 (8TDP.pdb) to the hydroperoxo intermediates in heme-dependent tyrosine hydroxylase[14] (7KQU.pdb), lactoperoxidase[15] (7DLQ.pdb), and a trapped oxygen adduct in the resting state CYP121 without cYY[47] (1N40.pdb). The Fe−O−O coordination angles for the end-on hydroperoxo intermediates are more significant (greater than 130°) compared to a smaller angle (105.3°) in CYP121 ferric-hydroperoxo, which is an indicative of a near side-on geometry relative to the heme iron. The $2F_0-F_c$ electron density maps (gray) for the heme ligand are contoured at 1 σ, the hemes are shown in pink, and the hydroperyxl ligand is in red.

the axial ligand. CYP121 has a much more pronounced heme ruffle compared to the more planar heme in TyrH and lactoperoxidase (Figure S17). The distal oxygen, which is 3.2 Å from the heme, is 3.1 Å from the phenol oxygen and 3.1 Å from the C3 (ortho to the hydroxy group) of the aromatic ring (Figure S8A), likely a stabilizing factor that allows for the accumulation of the intermediate, ultimately leading to its structural characterization.

The orientation of the hydroperoxo ligand and its proximity to the substrate hydroxy group affect the electron movement, which dictates the following intermediate in the catalytic cycle and whether it is sufficiently oxidizing to oxidize the substrate. The peroxo geometry has been directly shown, or indirectly implicated, to dictate the chemistry in a number of nonheme mononuclear iron enzymes.[66−68] While P450s typically use cpd I as the active oxidant, there is evidence that cpd 0 can drive oxidation reactions,[69] such as in sulfoxidation and *N*-dealkylation by P450 BM3[70] and olefin epoxidation by P450cam.[71] The P450cam mutant T252A demonstrates that disruption of the proton delivery network in the active site forces the enzyme to use an intermediate other than cpd I to oxidize its substrate.[8,71] Without delivery of a second H^+ to the distal oxygen of the hydroperoxo ligand, the high-valent ferryl species cannot be formed, yet epoxidation of the substrate was detected. It is worth mentioning that the ferric-hydroperoxo intermediate as the active oxidant for substrate oxidation has already previously been implicated to initiate substrate oxidation in fatty acid-metabolizing P450s, such as CYP5, CYP8A, and CYP74.[72−74] Comparison of our newly obtained 1.65 Å resolution CYP121 ES complex SFX-XFEL structure to the active site architecture of 20 representative P450s (Table S3) indicates that the proton delivery network is prevalent in this enzyme family. However, CYP121 is irregular in this respect. The glutamate or aspartate residue is occupied by a nonpolar isoleucine, and the terminal threonine, which delivers the proton to initiate cpd I formation, is a serine (Figure S18). In conjunction with these residue differences, CYP121 contains an arginine, known to stabilize well-ordered water molecules in the active site and to weakly interact with the tyrosyl moiety of cYY, which resides in an area that is vacant or is generally occupied by a nonpolar residue such as valine or leucine in other P450s. This indicates that CYP121 likely does not contain an efficient or effective proton delivery network to facilitate the protonation of cpd 0 for the O−O bond cleavage and cpd I formation and, instead, must rely upon its substrate cYY to provide a hydrogen atom.

Similarly, the C−C coupling mechanism mediated by CYP121 potentially uses the cpd 0 intermediate as the active oxidizing species rather than as a prerequisite to prepare for cpd I formation (Scheme 1B). The atypical end-on, which is near side-on, orientation of the hydroperoxo ligand positions itself differently from any known heme-based cpd 0 intermediate, orienting the distal oxygen approximately 3 Å from the substrate hydroxy group, priming it for hydrogen atom abstraction and homolytic cleavage of the O−O bond to form cpd II, which then oxidizes the substrate for a second time for diradical formation and eventual C−C coupling (Figure S19). The formation of cpd II as the second oxidizing species has now been corroborated by using hydrogen peroxide as the oxidant and observing an EPR-silent species forming and decaying over a period of one second, along with a concomitant formation and decay of a minor organic radical species. These findings are consistent with the "CYP121 peroxidase" denotation and proposed single electron transfer (SET) processes described in an earlier report,[19] and especially the previous finding that activation of the phenolic O−H, rather than a C−H bond, is critical for CYP121 reaction.[20] Since its discovery, CYP121 has been a mechanistic outlier in the P450 catalytic family because it remains predominantly low spin upon substrate binding, setting it apart from most of its superfamily. Therefore, the oxygen activation strategy at early steps, especially the active oxidant, becomes a central focus for studying the CYP121 catalytic mechanism.

CONCLUSIONS

In this work, we describe a rapid-mixing method for enzymatic reactions in single crystals with a case study. This method enables the serial femtosecond (SFX) crystallography to directly access milliseconds time domains at room temperature without freezing at any step of the structural determination. As a result, a long-sought P450-based ferric-hydroperoxo intermediate bound with the native substrate was structurally observed in situ after the 200 ms *in crystallo* reaction using this technology. This cpd 0 is the first of its kind characterized in a thiol-ligated heme-based enzyme.

The unprecedented high-spin intermediate after addition of an oxidant to the ES complex previously proposed for a cpd 0 species is finally understood. This spectroscopically and structurally observed high-spin intermediate is best modeled as a unique hydroperoxo binding mode that deviates from the traditional end-on cpd 0 intermediates in other heme enzymes. Instead, the hydroperoxo ligand is found in a near-side-on binding mode, which is relatively weakly associated with the iron ion, resulting in an unexpected high-spin state. The distal oxygen is in close contact with one of the phenolic oxygens of the bound substrate, cYY, in the heme distal pocket. The intermediate structure obtained by tr-SFX-XFEL suggests that

https://doi.org/10.1021/jacs.3c04991
J. Am. Chem. Soc. 2023, 145, 25120−25133

the ferric-hydroperoxo intermediate could function as an active oxidant for cYY oxidation. However, further studies are needed to better understand the oxygen activation mechanism for the noncanonical C−C bond-forming reaction mediated by this P450 enzyme.

■ ASSOCIATED CONTENT

Data Availability Statement

The atomic coordinates and structure factors have been deposited in the Protein Data Bank, www.pdb.org, with the following accession codes: CYP121 + cYY (ES), no oxidant, 8TDQ; CYP121 + cYY 200 ms after peracetic acid addition, 8TDP. Raw diffraction data of these SFX-XFEL structures have been deposited in the Coherent X-ray Imaging database (www.cxidb.org), ID 222, DOI: 10.11577/2204603.

Supporting Information

The Supporting Information is available free of charge at https://pubs.acs.org/doi/10.1021/jacs.3c04991.

Additional data and figures including EPR simulations, structure modeling and refinement, comparison to ferric-peroxo/hydroperoxo model complexes, and pH-dependent studies, including Figures S1 to S19, Tables S1 to S3, and corresponding references cited (PDF)

■ AUTHOR INFORMATION

Corresponding Authors

Jan F. Kern − *Molecular Biophysics and Integrated Bioimaging Division, Lawrence Berkeley National Laboratory, Berkeley, California 94720, United States*; Email: jfkern@lbl.gov

Aimin Liu − *Department of Chemistry, University of Texas, San Antonio, Texas 78249, United States*; orcid.org/0000-0002-4182-8176; Email: Feradical@utsa.edu

Authors

Romie C. Nguyen − *Department of Chemistry, University of Texas, San Antonio, Texas 78249, United States*

Ian Davis − *Department of Chemistry, University of Texas, San Antonio, Texas 78249, United States*; orcid.org/0000-0002-1566-4972

Medhanjali Dasgupta − *Molecular Biophysics and Integrated Bioimaging Division, Lawrence Berkeley National Laboratory, Berkeley, California 94720, United States*; Present Address: Medhanjali Dasgupta: The Fred and Pamela Buffett Cancer Center, University of Nebraska Medical Center, Omaha, Nebraska 68198, United States

Yifan Wang − *Department of Chemistry, University of Texas, San Antonio, Texas 78249, United States*; Present Address: Yifan Wang: Department of Chemistry, University of Georgia, Athens, Georgia 30602, United States

Philipp S. Simon − *Molecular Biophysics and Integrated Bioimaging Division, Lawrence Berkeley National Laboratory, Berkeley, California 94720, United States*; orcid.org/0000-0002-2859-4475

Agata Butryn − *Diamond Light Source, Harwell Science and Innovation Campus, Didcot, Oxfordshire OX11 0DE, United Kingdom; Research Complex at Harwell, Rutherford Appleton Laboratory, Didcot, Oxfordshire OX11 0FA, United Kingdom*; orcid.org/0000-0002-5227-4770

Hiroki Makita − *Molecular Biophysics and Integrated Bioimaging Division, Lawrence Berkeley National Laboratory, Berkeley, California 94720, United States*

Isabel Bogacz − *Molecular Biophysics and Integrated Bioimaging Division, Lawrence Berkeley National Laboratory, Berkeley, California 94720, United States*; orcid.org/0000-0003-1493-3867

Kednerlin Dornevil − *Department of Chemistry, University of Texas, San Antonio, Texas 78249, United States*; Present Address: Kednerlin Dornevil: Eurofins PSS, Indianapolis, Indiana 46202, United States

Pierre Aller − *Diamond Light Source, Harwell Science and Innovation Campus, Didcot, Oxfordshire OX11 0DE, United Kingdom; Research Complex at Harwell, Rutherford Appleton Laboratory, Didcot, Oxfordshire OX11 0FA, United Kingdom*; orcid.org/0000-0002-1793-7030

Asmit Bhowmick − *Molecular Biophysics and Integrated Bioimaging Division, Lawrence Berkeley National Laboratory, Berkeley, California 94720, United States*; orcid.org/0000-0002-6154-6635

Ruchira Chatterjee − *Molecular Biophysics and Integrated Bioimaging Division, Lawrence Berkeley National Laboratory, Berkeley, California 94720, United States*

In-Sik Kim − *Molecular Biophysics and Integrated Bioimaging Division, Lawrence Berkeley National Laboratory, Berkeley, California 94720, United States*

Tiankun Zhou − *Diamond Light Source, Harwell Science and Innovation Campus, Didcot, Oxfordshire OX11 0DE, United Kingdom; Research Complex at Harwell, Rutherford Appleton Laboratory, Didcot, Oxfordshire OX11 0FA, United Kingdom*

Derek Mendez − *Molecular Biophysics and Integrated Bioimaging Division, Lawrence Berkeley National Laboratory, Berkeley, California 94720, United States*

Daniel W. Paley − *Molecular Biophysics and Integrated Bioimaging Division, Lawrence Berkeley National Laboratory, Berkeley, California 94720, United States*

Franklin Fuller − *LCLS, SLAC National Accelerator Laboratory, Menlo Park, California 94025, United States*

Roberto Alonso Mori − *LCLS, SLAC National Accelerator Laboratory, Menlo Park, California 94025, United States*; orcid.org/0000-0002-5357-0934

Alexander Batyuk − *LCLS, SLAC National Accelerator Laboratory, Menlo Park, California 94025, United States*; orcid.org/0000-0002-9393-2880

Nicholas K. Sauter − *Molecular Biophysics and Integrated Bioimaging Division, Lawrence Berkeley National Laboratory, Berkeley, California 94720, United States*; orcid.org/0000-0003-2786-6552

Aaron S. Brewster − *Molecular Biophysics and Integrated Bioimaging Division, Lawrence Berkeley National Laboratory, Berkeley, California 94720, United States*; orcid.org/0000-0002-0908-7822

Allen M. Orville − *Diamond Light Source, Harwell Science and Innovation Campus, Didcot, Oxfordshire OX11 0DE, United Kingdom; Research Complex at Harwell, Rutherford Appleton Laboratory, Didcot, Oxfordshire OX11 0FA, United Kingdom*; orcid.org/0000-0002-7803-1777

Vittal K. Yachandra − *Molecular Biophysics and Integrated Bioimaging Division, Lawrence Berkeley National Laboratory, Berkeley, California 94720, United States*; orcid.org/0000-0002-3983-7858

Junko Yano − *Molecular Biophysics and Integrated Bioimaging Division, Lawrence Berkeley National Laboratory, Berkeley, California 94720, United States*; orcid.org/0000-0001-6308-9071

Complete contact information is available at:
https://pubs.acs.org/10.1021/jacs.3c04991

Notes

The authors declare no competing financial interest.

■ ACKNOWLEDGMENTS

The authors acknowledge the financial support of this work from the Lutcher Brown Endowment fund and Welch Foundation grant AX-2110-20220331 (to A.L.), the Presidential Distinguished Research Fellowship (to R.C.N.), the National Institutes of Health (NIH) grants GM108988 (to A.L.), GM117126 (to N.K.S.), GM55302 and GM149528 (to V.K.Y.), GM110501 (to J.Y.), GM126289 (to J.F.K.), and 1P41GM139687. The DOT instrument used in this research was funded by the Department of Energy (DOE), Office of Science, Office of Basic Energy Sciences (BES), Division of Chemical Sciences, Geosciences, and Biosciences (to J.F.K., J.Y., and V.K.Y.). Support for AMO was provided by a strategic grant 102593 jointly funded by the Wellcome Trust and Biotechnology and Biological Sciences Research Council (via James Naismith), Wellcome Investigator Award in Science 210734/Z/18/Z, Royal Society Wolfson Fellowship RSWF \R2\182017, and Biotechnology and Biological Sciences Research Council grant BB/V001892/1. This research used resources of NERSC, a User Facility supported by the Office of Science, DOE, under contract no. DE-AC02-05CH11231. XFEL data were collected at LCLS/SLAC, Stanford, under proposals LU50, LV43, P112, and P199A. The Rayonix detector used at LCLS was supported by the NIH grant S10 OD023453. Use of the LCLS, SLAC National Accelerator Laboratory, is supported by the U.S. DOE, Office of Science, OBES, under contract no. DE-AC02-76SF00515. We thank Kyle D. Sutherlin, Cindy C. Pham, and Sheraz Gul for support during experiment LU50 and Robert Bosman and Jos J.A.G. Kamps for support and discussions during experiment LV43.

■ REFERENCES

(1) Huang, X.; Groves, J. T. Oxygen activation and radical transformations in heme proteins and metalloporphyrins. *Chem. Rev.* **2018**, *118*, 2491−2553.
(2) Kühnel, K.; Derat, E.; Terner, J.; Shaik, S.; Schlichting, I. Structure and quantum chemical characterization of chloroperoxidase compound 0, a common reaction intermediate of diverse heme enzymes. *Proc. Natl. Acad. Sci. U. S. A.* **2007**, *104*, 99−104.
(3) Rittle, J.; Green, M. T. Cytochrome P450 compound I: capture, characterization, and C−H bond activation kinetics. *Science* **2010**, *330*, 933−937.
(4) Jin, S.; Bryson, T. A.; Dawson, J. H. Hydroperoxoferric heme intermediate as a second electrophilic oxidant in cytochrome P450-catalyzed reactions. *J. Biol. Inorg. Chem.* **2004**, *9*, 644−653.
(5) Mak, P. J.; Gregory, M. C.; Denisov, I. G.; Sligar, S. G.; Kincaid, J. R. Unveiling the crucial intermediates in androgen production. *Proc. Natl. Acad. Sci. U. S. A.* **2015**, *112*, 15856−15861.
(6) Woodward, J. J.; Chang, M. M.; Martin, N. I.; Marletta, M. A. The second step of the nitric oxide synthase reaction: Evidence for ferric-peroxo as the active oxidant. *J. Am. Chem. Soc.* **2009**, *131*, 297−305.
(7) Denisov, I. G.; Makris, T. M.; Sligar, S. G. Formation and decay of hydroperoxo-ferric heme complex in horseradish peroxidase studied by cryoradiolysis. *J. Biol. Chem.* **2002**, *277*, 42706−42710.
(8) Jin, S.; Makris, T. M.; Bryson, T. A.; Sligar, S. G.; Dawson, J. H. Epoxidation of olefins by hydroperoxo-ferric cytochrome P450. *J. Am. Chem. Soc.* **2003**, *125*, 3406−3407.
(9) Denisov, I. G.; Dawson, J. H.; Hager, L. P.; Sligar, S. G. The ferric-hydroperoxo complex of chloroperoxidase. *Biochem. Biophys. Res. Commun.* **2007**, *363*, 954−958.
(10) Unno, M.; Chen, H.; Kusama, S.; Shaik, S.; Ikeda-Saito, M. Structural characterization of the fleeting ferric peroxo species in myoglobin: Experiment and theory. *J. Am. Chem. Soc.* **2007**, *129*, 13394−13395.
(11) Hersleth, H.; Hsiao, Y.; Ryde, U.; Görbitz, C. H.; Andersson, K. K. The crystal structure of peroxymyoglobin generated through cryoradiolytic reduction of myoglobin compound III during data collection. *Biochem. J.* **2008**, *412*, 257−264.
(12) Petrik, I. D.; Davydov, R.; Ross, M.; Zhao, X.; Hoffman, B.; Lu, Y. Spectroscopic and crystallographic evidence for the role of a water-containing H-bond network in oxidase activity of an engineered myoglobin. *J. Am. Chem. Soc.* **2016**, *138*, 1134−1137.
(13) Mak, P. J.; Duggal, R.; Denisov, I. G.; Gregory, M. C.; Sligar, S. G.; Kincaid, J. R. Human cytochrome CYP17A1: The structural basis for compromised lyase activity with 17-hydroxyprogesterone. *J. Am. Chem. Soc.* **2018**, *140*, 7324−7331.
(14) Wang, Y.; Davis, I.; Shin, I.; Xu, H.; Liu, A. Molecular rationale for partitioning between C-H and C-F bond activation in heme-dependent tyrosine hydroxylase. *J. Am. Chem. Soc.* **2021**, *143*, 4680−4693.
(15) Singh, P. K.; Sharma, P.; Bhushan, A.; Kaur, P.; Sharma, S.; Singh, T. P. Structure of a ternary complex of lactoperoxidase with iodide and hydrogen peroxide at 1.77 Å resolution. *J. Inorg. Biochem.* **2021**, *220*, 111461−111469.
(16) Belin, P.; Le Du, M. H.; Fielding, A.; Lequin, O.; Jacquet, M.; Charbonnier, J. B.; Lecoq, A.; Thai, R.; Courçon, M.; Masson, C.; Dugave, C.; Genet, R.; Pernodet, J. L.; Gondry, M. Identification and structural basis of the reaction catalyzed by CYP121, an essential cytochrome P450 in *Mycobacterium tuberculosis*. *Proc. Natl. Acad. Sci. U. S. A.* **2009**, *106*, 7426−7431.
(17) McLean, K. J.; Carroll, P.; Lewis, D. G.; Dunford, A. J.; Seward, H. E.; Neeli, R.; Cheesman, M. R.; Marsollier, L.; Douglas, P.; Smith, W. E.; Rosenkrands, I.; Cole, S. T.; Leys, D.; Parish, T.; Munro, A. W. Characterization of active site structure in CYP121. A cytochrome P450 essential for viability of *Mycobacterium tuberculosis* H37Rv. *J. Biol. Chem.* **2008**, *283*, 33406−33416.
(18) Ortiz de Montellano, P. R. Potential drug targets in the *Mycobacterium tuberculosis* cytochrome P450 system. *J. Biol. Inorg. Chem.* **2018**, *180*, 235−245.
(19) Dornevil, K.; Davis, I.; Fielding, A. J.; Terrell, J. R.; Liu, A. Crosslinking of dicyclotyrosine by the cytochrome P450 enzyme CYP121 from *Mycobacterium tuberculosis* proceeds through a catalytic shunt pathway. *J. Biol. Chem.* **2017**, *292*, 13645−13657.
(20) Nguyen, R. C.; Yang, Y.; Wang, Y.; Davis, I.; Liu, A. Substrate-assisted hydroxylation and *O*-demethylation in the peroxidase-like cytochrome P450 enzyme CYP121. *ACS Catal.* **2020**, *10*, 1628−1639.
(21) Fielding, A. J.; Dornevil, K.; Ma, L.; Davis, I.; Liu, A. Probing ligand exchange in the P450 enzyme CYP121 from *Mycobacterium tuberculosis*: Dynamic equilibrium of the distal heme ligand as a function of pH and temperature. *J. Am. Chem. Soc.* **2017**, *139*, 17484−17499.
(22) Greenspan, F. P.; MacKellar, D. G. Analysis of aliphatic per acids. *Anal. Chem.* **1948**, *20*, 1061−1063.
(23) Rajput, S.; McLean, K. J.; Poddar, H.; Selvam, I. R.; Nagalingam, G.; Triccas, J. A.; Levy, C. W.; Munro, A. W.; Hutton, C. A. Structure−activity relationships of cyclo(L-tyrosyl-L-tyrosine) derivatives binding to *Mycobacterium tuberculosis* CYP121: Iodinated analogues promote shift to high-spin adduct. *J. Med. Chem.* **2019**, *62*, 9792−9805.
(24) Fuller, F. D.; Gul, S.; Chatterjee, R.; Burgie, E. S.; Young, I. D.; Lebrette, H.; Srinivas, V.; Brewster, A. S.; Michels-Clark, T.; Clinger, J. A.; Andi, B.; Ibrahim, M.; Pastor, E.; de Lichtenberg, C.; Hussein, R.; Pollock, C. J.; Zhang, M.; Stan, C. A.; Kroll, T.; Fransson, T.; Weninger, C.; Kubin, M.; Aller, P.; Lassalle, L.; Bräuer, P.; Miller, M. D.; Amin, M.; Koroidov, S.; Roessler, C. G.; Allaire, M.; Sierra, R. G.; Docker, P. T.; Glownia, J. M.; Nelson, S.; Koglin, J. E.; Zhu, D.;

Chollet, M.; Song, S.; Lemke, H.; Liang, M.; Sokaras, D.; Alonso-Mori, R.; Zouni, A.; Messinger, J.; Bergmann, U.; Boal, A. K.; Bollinger, J. M.; Krebs, C.; Högbom, M.; Phillips, G. N.; Vierstra, R. D.; Sauter, N. K.; Orville, A. M.; Kern, J.; Yachandra, V. K.; Yano, J. Drop-on-demand sample delivery for studying biocatalysts in action at X-ray free-electron lasers. *Nat. Methods* **2017**, *14*, 443−449.
(25) Butryn, A.; Simon, P. S.; Aller, P.; Hinchliffe, P.; Massad, R. N.; Leen, G.; Tooke, C. L.; Bogacz, I.; Kim, I. S.; Bhowmick, A.; Brewster, A. S.; Devenish, N. E.; Brem, J.; Kamps, J.; Lang, P. A.; Rabe, P.; Axford, D.; Beale, J. H.; Davy, B.; Ebrahim, A.; Orlans, J.; Storm, S.; Zhou, T.; Owada, S.; Tanaka, R.; Tono, K.; Evans, G.; Owen, R. L.; Houle, F. A.; Sauter, N. K.; Schofield, C. J.; Spencer, J.; Yachandra, V. K.; Yano, J.; Kern, J. F.; Orville, A. M. An on-demand, drop-on-drop method for studying enzyme catalysis by serial crystallography. *Nat. Commun.* **2021**, *12*, 4461−4468.
(26) Campomizzi, C. S.; Ghanatios, G. E.; Estrada, D. F. ^{19}F-NMR reveals substrate specificity of CYP121A1 in *Mycobacterium tuberculosis*. *J. Biol. Chem.* **2021**, *297*, No. 101287.
(27) Kumar, A.; Campomizzi, C. S.; Jay, N.; Ferguson, S.; Scheffler, E. J.; Lioi, J.; Tu, C.; Qu, J.; Simons, C.; Estrada, D. F. Surface hydrophobics mediate functional dimerization of CYP121A1 of *Mycobacterium tuberculosis*. *Sci. Rep.* **2021**, *11*, 394.
(28) Campomizzi, C. S.; Kumar, A.; Uttamrao, P. P.; Stallone, J. J.; Ghanatios, G. E.; Rathinavelan, T.; Estrada, D. F. Active site aromatic residues play a dual role in the substrate interaction and protein structure in functional dimers of CYP121A1 of *Mycobacterium tuberculosis*. *ACS Infect. Dis.* **2023**, *9*, 827−839.
(29) Njuma, O. J.; Davis, I.; Ndontsa, E. N.; Krewall, J. R.; Liu, A.; Goodwin, D. C. Mutual synergy between catalase and peroxidase activities of the bifunctional enzyme KatG is facilitated by electron hole-hopping within the enzyme. *J. Biol. Chem.* **2017**, *292*, 18408−18421.
(30) Stoll, S.; Schweiger, A. EasySpin, a comprehensive software package for spectral simulation and analysis in EPR. *J. Magn. Reson.* **2006**, *178*, 42−55.
(31) Brewster, A. S.; Young, I. D.; Lyubimov, A.; Bhowmick, A.; Sauter, N. K. Processing serial crystallographic data from XFELs or synchrotrons using the cctbx.xfel GUI. *Comput. Crystallogr. Newsl.* **2019**, *10*, 22−39.
(32) Hattne, J.; Echols, N.; Tran, R.; Kern, J.; Gildea, R. J.; Brewster, A. S.; Alonso-Mori, R.; Glöckner, C.; Hellmich, J.; Laksmono, H.; Sierra, R. G.; Lassalle-Kaiser, B.; Lampe, A.; Han, G.; Gul, S.; DiFiore, D.; Milathianaki, D.; Fry, A. R.; Miahnahri, A.; White, W. E.; Schafer, D. W.; Seibert, M. M.; Koglin, J. E.; Sokaras, D.; Weng, T.-C.; Sellberg, J.; Latimer, M. J.; Glatzel, P.; Zwart, P. H.; Grosse-Kunstleve, R. W.; Bogan, M. J.; Messerschmidt, M.; Williams, G. J.; Boutet, S.; Messinger, J.; Zouni, A.; Yano, J.; Bergmann, U.; Yachandra, V. K.; Adams, P. D.; Sauter, N. K. Accurate macromolecular structures using minimal measurements from X-ray free-electron lasers. *Nat. Methods* **2014**, *11*, 545−548.
(33) Sauter, N. K. XFEL diffraction: Developing processing methods to optimize data quality. *J. Synchrotron Radiat.* **2015**, *22*, 239−248.
(34) Sauter, N. K.; Hattne, J.; Brewster, A. S.; Echols, N.; Zwart, P. H.; Adams, P. D. Improved crystal orientation and physical properties from single-shot XFEL stills. *Acta Crystallogr., Sect. D: Biol. Crystallogr.* **2014**, *70*, 3299−3309.
(35) Brewster, A. S.; Bhowmick, A.; Bolotovsky, R.; Mendez, D.; Zwart, P. H.; Sauter, N. K. SAD phasing of XFEL data depends critically on the error model. *Acta Crystallogr., Sect. D: Struct. Biol.* **2019**, *75*, 959−968.
(36) Winter, G.; Waterman, D. G.; Parkhurst, J. M.; Brewster, A. S.; Gildea, R. J.; Gerstel, M.; Fuentes-Montero, L.; Vollmar, M.; Michels-Clark, T.; Young, I. D.; Sauter, N. K.; Evans, G. DIALS: Implementation and evaluation of a new integration package. *Acta Crystallogr., Sect. D: Struct. Biol.* **2018**, *74*, 85−97.
(37) Adams, P. D.; Afonine, P. V.; Bunkoczi, G.; Chen, V. B.; Davis, I. W.; Echols, N.; Headd, J. J.; Hung, L.-W.; Kapral, G. J.; Grosse-Kunstleve, R. W.; McCoy, A. J.; Moriarty, N. W.; Oeffner, R.; Read, R. J.; Richardson, D. C.; Richardson, J. S.; Terwilliger, T. C.; Zwart, P. H. Phenix: a comprehensive Python-based system for macromolecular structure solution. *Acta Crystallogr., Sect. D: Biol. Crystallogr.* **2010**, *66*, 213−221.
(38) Wang, Y.; Liu, K. F.; Yang, Y.; Davis, I.; Liu, A. Observing 3-hydroxyanthranilate-3,4-dioxygenase in action through a crystalline lens. *Proc. Natl. Acad. Sci. U. S. A.* **2020**, *117*, 19720−19730.
(39) Schmidt, M. Reaction initiation in enzyme crystals by diffusion of substrate. *Crystals* **2020**, *10*, 116−131.
(40) Huo, L.; Davis, I.; Liu, F.; Andi, B.; Esaki, S.; Iwaki, H.; Hasegawa, Y.; Orville, A. M.; Liu, A. Crystallographic and spectroscopic snapshots reveal a dehydrogenase in action. *Nat. Commun.* **2015**, *6*, 5935.
(41) Lang, P. T.; Holton, J. M.; Fraser, J. S.; Alber, T. Protein structural ensembles are revealed by redefining X-ray electron density noise. *Proc. Natl. Acad. Sci. U. S. A.* **2014**, *111*, 237−242.
(42) Burstyn, J. N.; Roe, J. A.; Miksztal, A. R.; Shaevitz, B. A.; Lang, G.; Valentine, J. S. Magnetic and spectroscopic characterization of an iron porphyrin peroxide complex. Peroxoferrioctaethylporphyrin (1-). *J. Am. Chem. Soc.* **1988**, *110*, 1382−1388.
(43) Chufán, E. E.; Karlin, K. D. An iron−peroxo porphyrin complex: New synthesis and reactivity toward a Cu(II) complex giving a heme−peroxo−copper adduct. *J. Am. Chem. Soc.* **2003**, *125*, 16160−16161.
(44) Gallagher, A. T.; Lee, J. Y.; Kathiresan, V.; Anderson, J. S.; Hoffman, B. M.; Harris, T. D. A structurally-characterized peroxomanganese(IV) porphyrin from reversible O_2 binding within a metal−organic framework. *Chem. Sci.* **2018**, *9*, 1596−1603.
(45) Gosiewska, S.; van Faassen, E. E.; Permentier, H. P.; Bruins, A. P.; van Koten, G.; Klein Gebbink, R. J. M. Characterization and alkane oxidation activity of a diastereopure seven-coordinate iron(III) alkylperoxo complex. *Dalton Trans.* **2007**, 3365−3368.
(46) Liu, J. G.; Ohta, T.; Yamaguchi, S.; Ogura, T.; Sakamoto, S.; Maeda, Y.; Naruta, Y. Spectroscopic characterization of a hydroperoxo-heme intermediate: conversion of a side-on peroxo to an end-on hydroperoxo complex. *Angew. Chem., Int. Ed. Engl.* **2009**, *48*, 9262−9267.
(47) Liu, J. G.; Shimizu, Y.; Ohta, T.; Naruta, Y. Formation of an end-on ferric-peroxo intermediate upon one-electron reduction of a ferric superoxo heme. *J. Am. Chem. Soc.* **2010**, *132*, 3672−3673.
(48) VanAtta, R. B.; Strouse, C. E.; Hanson, L. K.; Valentine, J. S. Peroxo(tetraphenylporphinato)manganese(III) and chloro(tetraphenylporphinato)manganese(II) anions. Synthesis, crystal structures, and electronic structures. *J. Am. Chem. Soc.* **1987**, *109*, 1425−1434.
(49) Leys, D.; Mowat, C. G.; McLean, K. J.; Richmond, A.; Chapman, S. K.; Walkinshaw, M. D.; Munro, A. W. Atomic structure of *Mycobacterium tuberculosis* CYP121 to 1.06 Å reveals novel features of cytochrome P450. *J. Biol. Chem.* **2003**, *278*, 5141−5147.
(50) Melik-Adamyan, W.; Bravo, J.; Carpena, X.; Switala, J.; Maté, M. J.; Fita, I.; Loewen, P. C. Substrate flow in catalases deduced from the crystal structures of active site variants of HPII from *Escherichia coli*. *Proteins* **2001**, *44*, 270−281.
(51) Namuswe, F.; Kasper, G. D.; Sarjeant, A. N.; Hayashi, T.; Krest, C. M.; Green, M. T.; Moënne-Loccoz, P.; Goldberg, D. P. Rational tuning of the thiolate donor in model complexes of superoxide reductase: Direct evidence for a *trans* influence in Fe^{III}−OOR complexes. *J. Am. Chem. Soc.* **2008**, *130*, 14189−14200.
(52) Davydov, R.; Hoffman, B. M. Active intermediates in heme monooxygenase reactions as revealed by cryoreduction/annealing, EPR/ENDOR studies. *Arch. Biochem. Biophys.* **2011**, *507*, 36−43.
(53) Davydov, R.; Makris, T. M.; Kofman, V.; Werst, D. E.; Sligar, S. G.; Hoffman, B. M. Hydroxylation of camphor by reduced oxy-cytochrome P450cam: Mechanistic implications of EPR and ENDOR studies of catalytic intermediates in native and mutant enzymes. *J. Am. Chem. Soc.* **2001**, *123*, 1403−1415.
(54) Davydov, R.; Razeghifard, R.; Im, S.-C.; Waskell, L.; Hoffman, B. M. Characterization of the microsomal cytochrome P450 2B4 O_2 activation intermediates by cryoreduction and electron paramagnetic resonance. *Biochemistry* **2008**, *47*, 9661−9666.

https://doi.org/10.1021/jacs.3c04991
J. Am. Chem. Soc. 2023, 145, 25120−25133

(55) Davydov, R.; Gilep, A. A.; Strushkevich, N. V.; Usanov, S. A.; Hoffman, B. M. Compound I is the reactive intermediate in the first monooxygenation step during conversion of cholesterol to pregnenolone by cytochrome P450scc: EPR/ENDOR/cryoreduction/annealing Studies. *J. Am. Chem. Soc.* **2012**, *134*, 17149−17156.
(56) Tsai, R.; Yu, C. A.; Gunsalus, I. C.; Peisach, J.; Blumberg, W.; Orme-Johnson, W. H.; Beinert, H. Spin-state changes in cytochrome P-450cam on binding of specific substrates. *Proc. Natl. Acad. Sci. U. S. A.* **1970**, *66*, 1157−1163.
(57) Davydov, R.; Im, S.; Shanmugam, M.; Gunderson, W. A.; Pearl, N. M.; Hoffman, B. M.; Waskell, L. Role of the proximal cysteine hydrogen bonding interaction in cytochrome P450 2B4 studied by cryoreduction, electron paramagnetic resonance, and electron−nuclear double resonance spectroscopy. *Biochemistry* **2016**, *55*, 869−883.
(58) Davydov, R.; Strushkevich, N.; Smil, D.; Yantsevich, A.; Gilep, A.; Usanov, S.; Hoffman, B. M. Evidence that compound I is the active species in both the hydroxylase and lyase steps by which P450scc converts cholesterol to pregnenolone: EPR/ENDOR/cryoreduction/annealing studies. *Biochemistry* **2015**, *54*, 7089−7097.
(59) Davydov, R.; Laryukhin, M.; Ledbetter-Rogers, A.; Sono, M.; Dawson, J. H.; Hoffman, B. M. Electron paramagnetic resonance and electron-nuclear double resonance studies of the reactions of cryogenerated hydroperoxoferric−hemoprotein intermediates. *Biochemistry* **2014**, *53*, 4894−4903.
(60) Zhao, X.; Ting, Z.; Yu-Jie, Z.; De-Hua, L. Preparation of peracetic acid from acetic acid and hydrogen peroxide: Experimentation and modeling. *Chin. J. Proc. Eng.* **2008**, *8*, 35−41.
(61) Dey, A.; Solomon, E. I. Density functional theory calculations on Fe−O and O−O cleavage of ferric hydroperoxide species: Role of axial ligand and spin state. *Inorg. Chim. Acta* **2010**, *363*, 2762−2767.
(62) Zaragoza, J. T.; Goldberg, D. P., Chapter 1 Dioxygen binding and activation mediated by transition metal porphyrinoid complexes. In *Dioxygen-dependent Heme Enzymes*; The Royal Society of Chemistry: 2019; pp 1−36.
(63) Sato, M.; Kon, H.; Kumaki, K.; Nebert, D. W. Comparative EPR study on high-spin ferric porphine complexes and cytochrome P450 having rhombic character. *Biochem. Biophys. Acta* **1977**, *498*, 403−421.
(64) Jiang, Y.; Telser, J.; Goldberg, D. P. Evidence for the formation of a mononuclear ferric−hydroperoxo complex via the reaction of dioxygen with an (N_4S(thiolate))iron(II) complex. *Chem. Commun.* **2009**, 6828−6830.
(65) Shearer, J.; Scarrow, R. C.; Kovacs, J. A. Synthetic models for the cysteinate-ligated non-heme iron enzyme superoxide reductase: Observation and structural characterization by XAS of an FeIII−OOH intermediate. *J. Am. Chem. Soc.* **2002**, *124*, 11709−11717.
(66) Kovaleva, E. G.; Lipscomb, J. D. Versatility of biological non-heme Fe(II) centers in oxygen activation reactions. *Nat. Chem. Biol.* **2008**, *4*, 186−193.
(67) Kal, S.; Que, L. Dioxygen activation by nonheme iron enzymes with the 2-His-1-carboxylate facial triad that generate high-valent oxoiron oxidants. *J. Biol. Inorg. Chem.* **2017**, *22*, 339−365.
(68) Solomon, E. I.; Decker, A.; Lehnert, N. Non-heme iron enzymes: Contrasts to heme catalysis. *Proc. Natl. Acad. Sci. U. S. A.* **2003**, *100*, 3589−3594.
(69) Vaz, A. D.; Pernecky, S. J.; Raner, G. M.; Coon, M. J. Peroxo-iron and oxenoid-iron species as alternative oxygenating agents in cytochrome P450-catalyzed reactions: Switching by threonine-302 to alanine mutagenesis of cytochrome P450 2B4. *Proc. Natl. Acad. Sci. U. S. A.* **1996**, *93*, 4644−4648.
(70) Volz, T. J.; Rock, D. A.; Jones, J. P. Evidence for two different active oxygen species in cytochrome P450 BM3 mediated sulfoxidation and N-dealkylation reactions. *J. Am. Chem. Soc.* **2002**, *124*, 9724−9725.
(71) Vaz, A. D.; McGinnity, D. F.; Coon, M. J. Epoxidation of olefins by cytochrome P450: Evidence from site-specific mutagenesis for hydroperoxo-iron as an electrophilic oxidant. *Proc. Natl. Acad. Sci. U. S. A.* **1998**, *95*, 3555−3560.
(72) Brash, A. R. Mechanistic aspects of CYP74 allene oxide synthases and related cytochrome P450 enzymes. *Phytochemistry* **2009**, *70*, 1522−1531.
(73) Cho, K. B.; Lai, W.; Hamberg, M.; Raman, C. S.; Shaik, S. The reaction mechanism of allene oxide synthase: Interplay of theoretical QM/MM calculations and experimental investigations. *Arch. Biochem. Biophys.* **2011**, *507*, 14−25.
(74) Boeglin, W. E.; Brash, A. R. Cytochrome P450-type hydroxylation and epoxidation in a tyrosine-liganded hemoprotein, catalase-related allene oxide synthase. *J. Biol. Chem.* **2012**, *287*, 24139−24147.

https://doi.org/10.1021/jacs.3c04991
J. Am. Chem. Soc. 2023, 145, 25120−25133

Supplementary Information

In situ Structural Observation of a Substrate- and Peroxide-Bound High-Spin Ferric-Hydroperoxo Intermediate in P450 Enzyme CYP121

Romie C. Nguyen,[1] Ian Davis,[1] Medhanjali Dasgupta,[2] Yifan Wang,[1†] Philipp S. Simon,[2‡] Agata Butryn,[3,4] Hiroki Makita,[2] Isabel Bogacz,[2] Kednerlin Dornevil,[1‡] Pierre Aller,[3,4] Asmit Bhowmick,[2] Ruchira Chatterjee,[2] In-Sik Kim,[2] Tiankun Zhou,[3,4] Derek Mendez,[2] Daniel W. Paley,[2] Franklin Fuller,[5] Roberto Alonso Mori,[5] Alexander Batyuk,[5] Nicholas K. Sauter,[2] Aaron S. Brewster,[2] Allen M. Orville,[3,4] Vittal K. Yachandra,[2] Junko Yano,[2] Jan F. Kern,[2,*] and Aimin Liu[1,*]

[1]Department of Chemistry, University of Texas, San Antonio, TX 78249, United States

[2]Molecular Biophysics and Integrated Bioimaging Division, Lawrence Berkeley National Laboratory, Berkeley, CA 94720, United States

[3]Diamond Light Source, Harwell Science and Innovation Campus, Didcot, Oxfordshire OX11 0DE, United Kingdom

[4]Research Complex at Harwell, Rutherford Appleton Laboratory, Didcot, Oxfordshire OX11 0FA, United Kingdom

[5]LCLS, SLAC National Accelerator Laboratory, Menlo Park, CA 94025, United States

*Corresponding authors: Aimin Liu and Jan F. Kern

E-mail: Feradical@utsa.edu or jfkern@lbl.gov

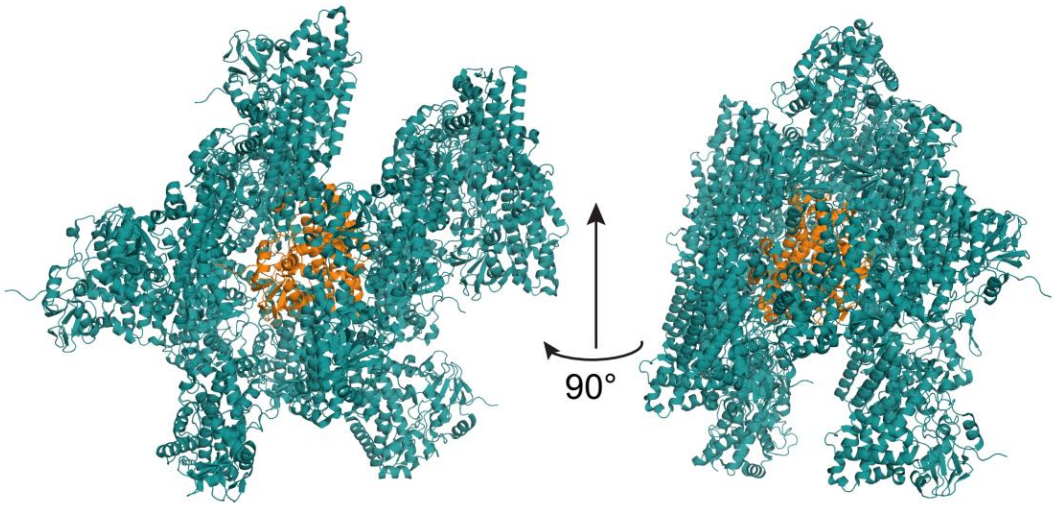

Figure S1. Cartoon representation of CYP121 packing in the crystal lattice. A monomer in the unit cell is shown in orange, and its symmetrical mates within 20 Å are shown in teal.

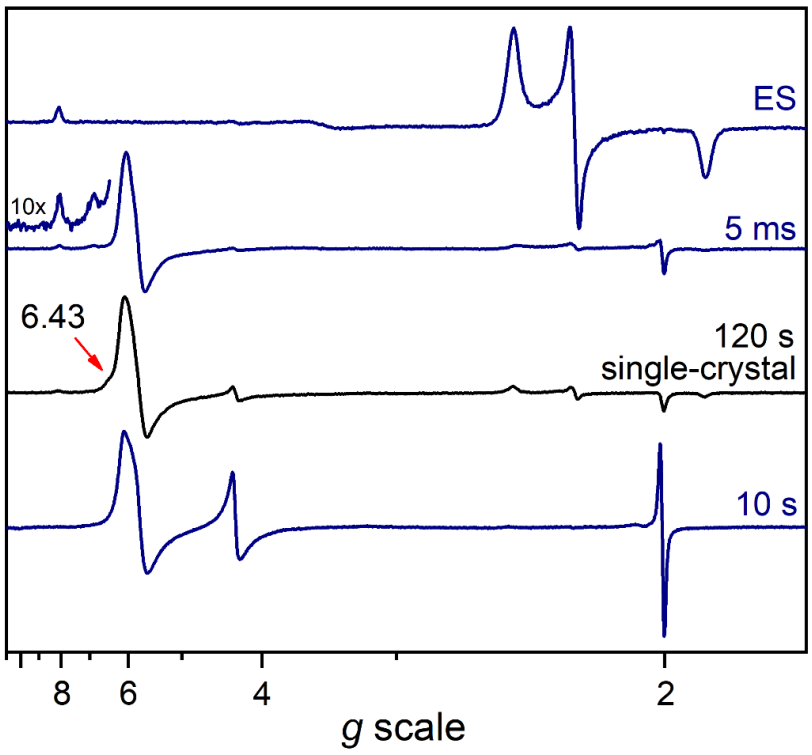

Figure S2. Solution state CYP121 ES complex reacting with 10 mM peracetic acid (PAA) in RFQ-EPR compared to single-crystal EPR of ES complex reacting with 5 mM PAA. RFQ-EPR spectra are navy, and the single-crystal EPR spectrum is black. Within 5 ms, a new partial rhombic high-spin intermediate was captured in the solution state.[1] A similar partial rhombic intermediate is also observed as a small shoulder on the axial high-spin signal at g = 6.43, 5.76, and 2.0 in single-crystal EPR within 120 s, with differences arising due to many crystals used with varying orientations in the EPR tube. This partial rhombic intermediate then decays to high-spin (axial S = 5/2 and isotropic S = 3/2) species observed in the 10 s spectrum due to the high concentration of PAA used to maximize the initial high-spin partial rhombic intermediate, and therefore is not a part of the catalytic mechanism.

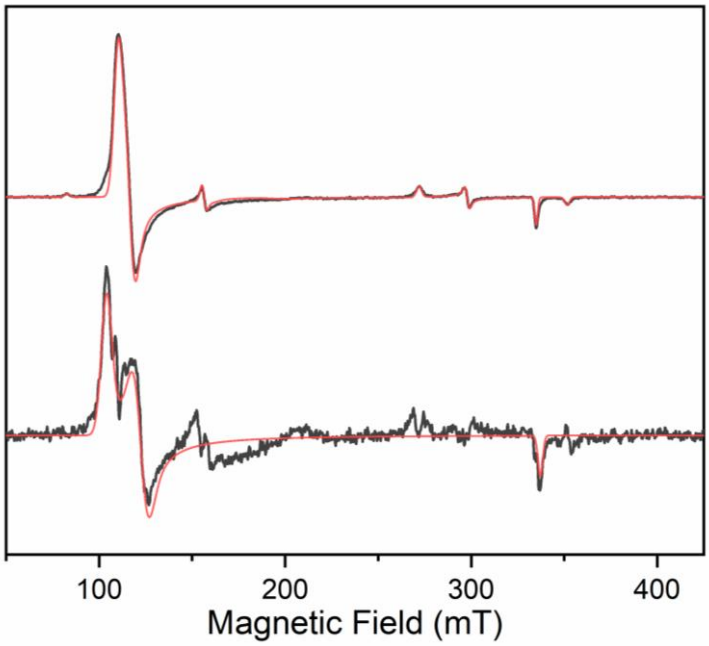

Figure S3. Simulation of the 120-s single-crystal EPR spectrum. The 120 s EPR spectrum (top, black) is overlaid with the simulation (top, red) of the high-spin signal (g = 5.76) as an axial 6-coordinate species, which results in an incomplete fit of the experimental data. The residuals (bottom, black) indicate the apparent presence of a smaller, rhombic high-spin signal. This rhombic signal can be simulated as a distinct and separate 6-coordinate high-spin intermediate (bottom, red).

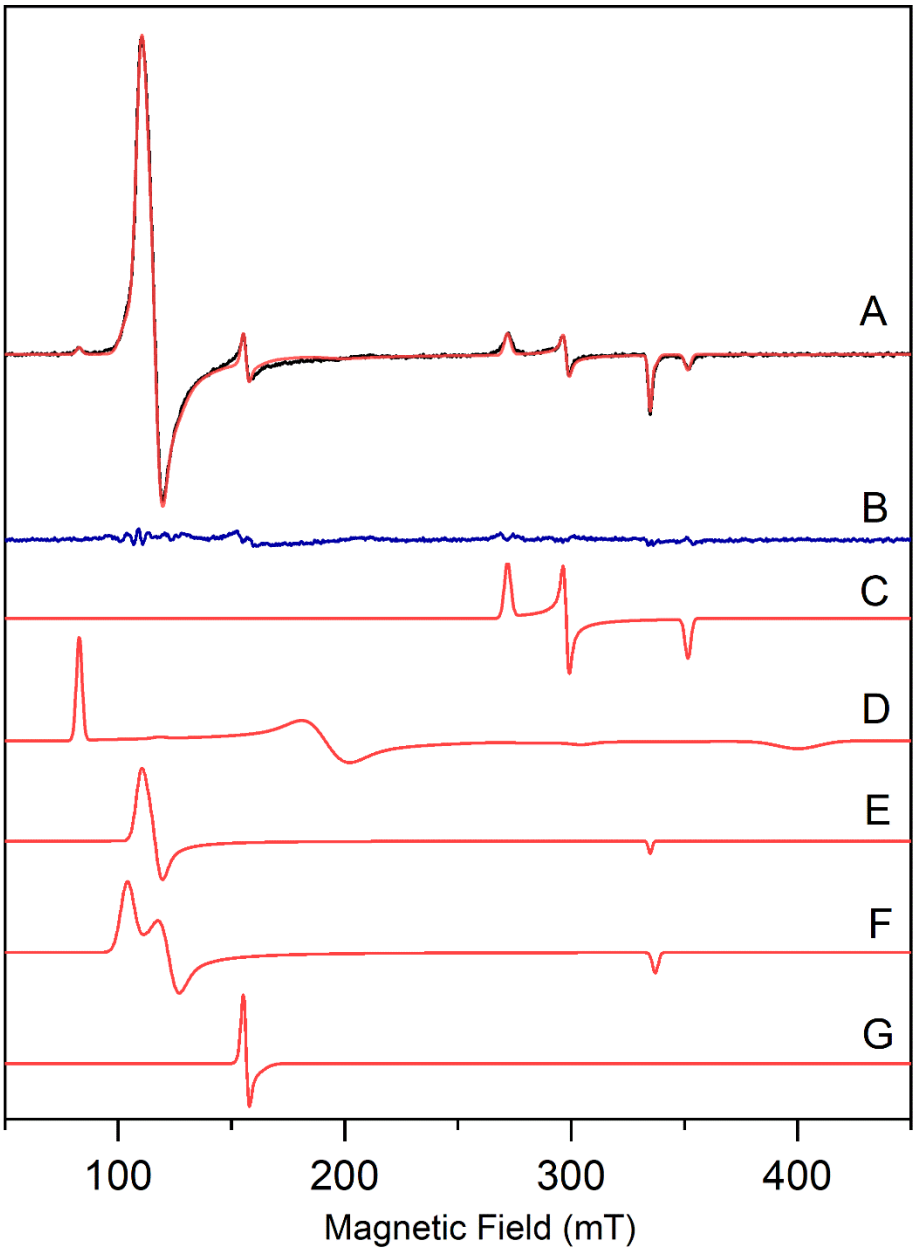

Figure S4. Full simulation of the 120 s EPR spectrum of ES complex single crystals reacting with 5 mM peracetic acid showing the different components present in the experimental data. (**A**) The 120 s EPR spectrum (black trace) with the full spectrum simulation is overlaid in red. (**B**) Residual after simulation of the 120 s spectrum indicates satisfactory fit of the experimental data. The following components were used to simulate the experimental data; (**C**) 6-coordinate low-spin, (**D**) 5-coordinate high-spin, (**E**) axial 6-coordinate high-spin, (**F**) rhombic 6-coordinate high-spin, and (**G**) isotropic high-spin at g = 4.27.

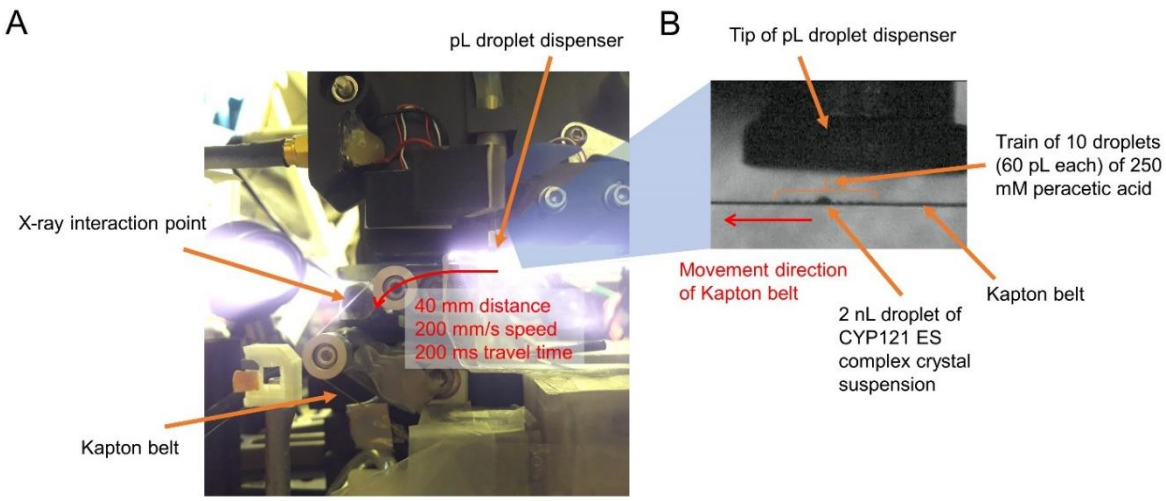

Figure S5. Setup for Drop-on-Tape mixing utilized in the room temperature SFX-XFEL data collection. (A) The picoliter droplet dispenser is positioned above the Kapton belt that transports nanoliter droplets of protein sample toward the X-ray interaction point. (B) The pL dispenser produces trains of droplets of 60 pL, each containing 250 mM peracetic acid. The bursts are timed such as that 2 out of the 10 droplets merge with the 2 nL drops of crystal suspension. The distance of 40 mm between the droplet merging point and the X-ray interaction point combined with a belt speed of 200 mm/s leads to a mixing time of 200 ms between the peracetic acid and the CYP121 ES complex crystal suspension before being probed by the X-rays.

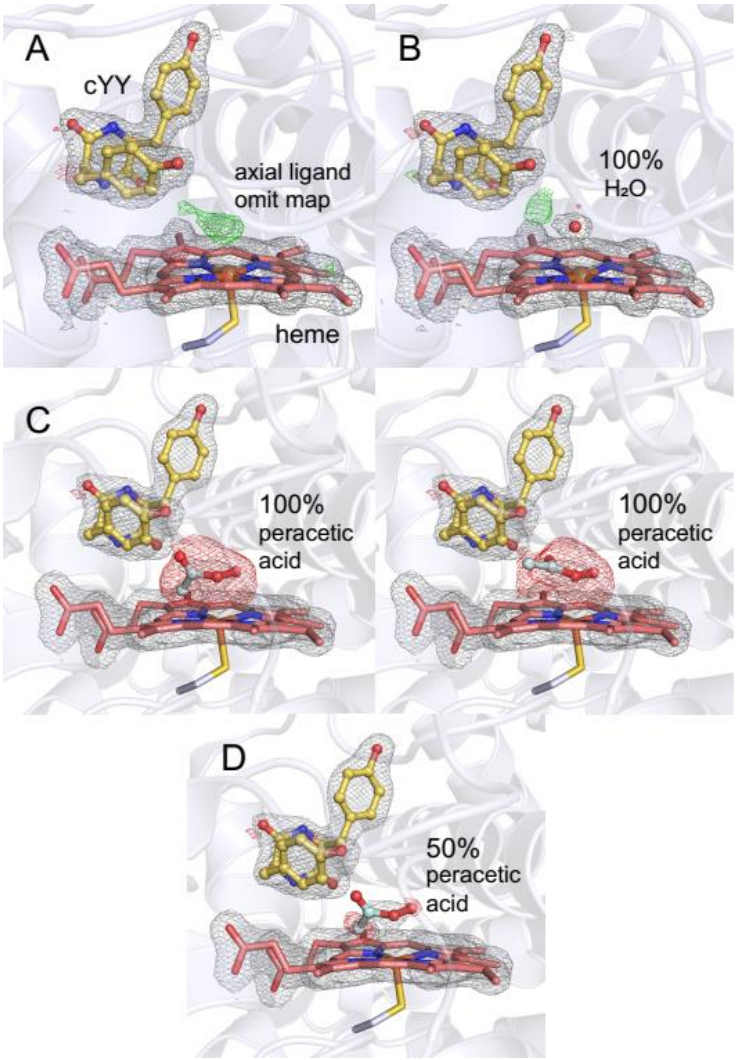

Figure S6. Room temperature SFX-XFEL crystal structure of CYP121 cocrystallized with cYY microcrystal slurry reacting with 14 mM peracetic acid for 200 ms reported at 1.85 Å resolution. The $2F_o$-F_c electron density map (gray) is contoured at 1 σ, and the F_o-F_c electron density map is contoured at 3 and -3 σ (green and red, respectively). (**A**), Omit map of the axial heme ligand. The shape of the density is oblong rather than spherical, which is unusual for a water/hydroxide ligand. (**B**), Refinement results after a water/hydroxide molecule is fitted into the ligand density. Excess positive density which appears as if it can accommodate an oxygen atom, is present next to the ligand, indicating that the electron density cannot be interpreted with a water/hydroxide ligand. (**C**) Refinement of a peracetic acid into the axial density at 100% occupancy using two separate orientations. Dreadful overfitting of the density is observed as a significant negative difference density (shown at -3 σ). (**D**) Reduction of occupancy to 50% for the peracetic acid ligand was attempted. Overfitting was still observed for the $-CH_3$ and -OH atoms, leading to the conclusion that peracetic acid is not observable in the active site. The ligand cYY is yellow, the heme is pink, the axial water is a red sphere, and peracetic acid is light cyan.

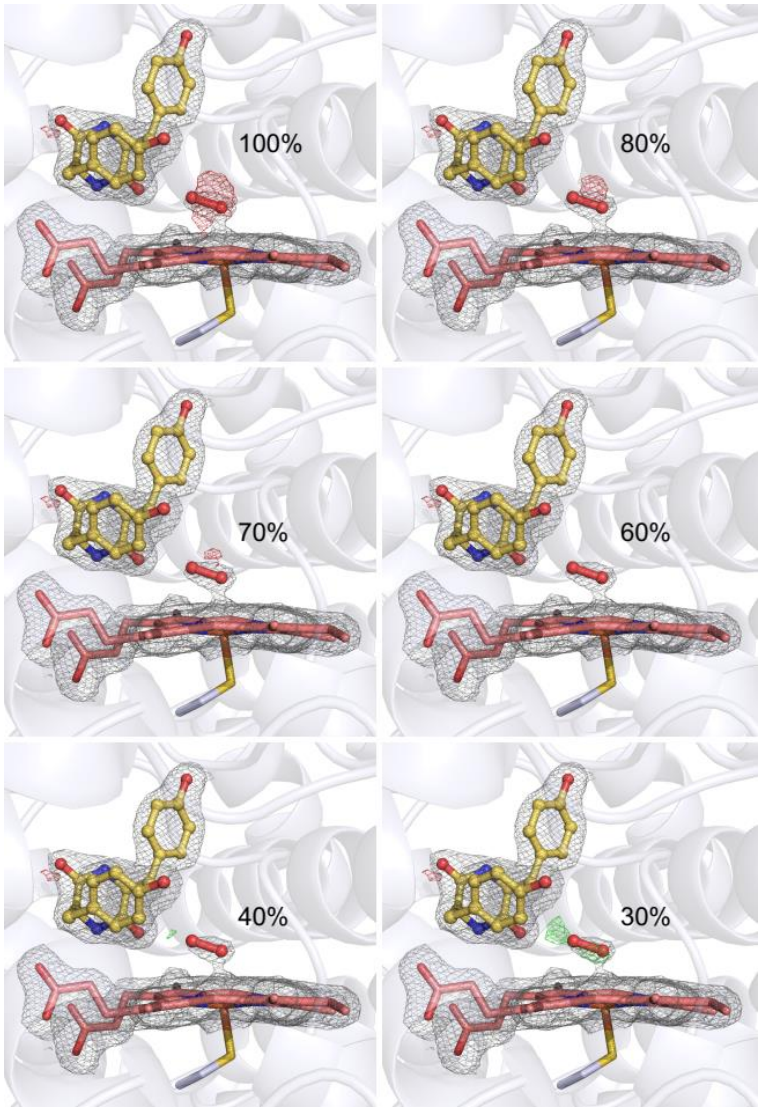

Figure S7. Refinement results for a peroxide ligand in the axial ligand density at varying occupancies in the ES complex reacting with peracetic acid for 200 ms (8TDP.pdb). Refinement of the axial peroxide ligand at full occupancy results in extensive overfitting as seen by the marked presence of red density. Overfitting of the ligand density decreases to 60%, with underfitted density (green) beginning to appear at 40% occupancy. The 60% occupancy structure was refined a step further in Phenix to allow the software to calculate optimal ligand occupancy, which resulted in 52% as shown in Figure 2 in the main text. The $2F_o$-F_c electron density map (gray) is contoured to 1 σ. The F_o-F_c density map (green and red) is contoured to 3 σ and -3 σ, respectively. Native substrate cYY is yellow, the heme is pink, and the peroxide ligand is red.

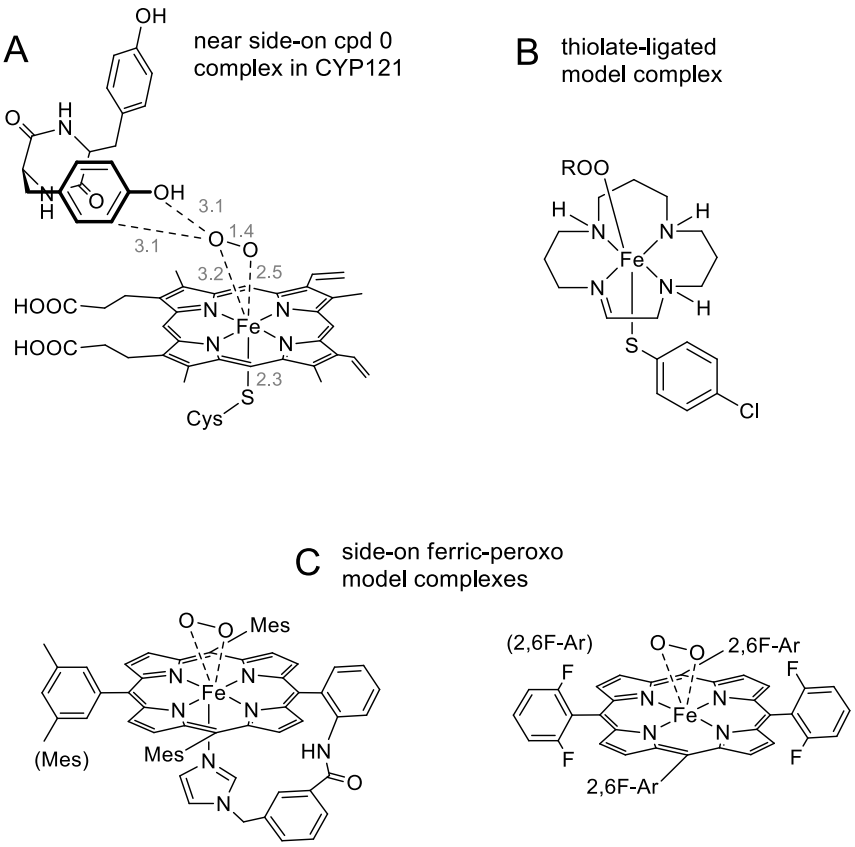

Figure S8. A two-dimensional chemical representation the cpd 0 intermediate in CYP121 compared to a thiolate-ligated ferric-hydroperoxo model complex and side-on peroxo model complexes. (**A**) Distances (Å) are measured for the CYP121 ferric-peroxo/hydroperoxo intermediate from the peroxo/hydroperoxyl ligand to the heme iron and substrate cYY. (**B**) Thiolate-ligated ferric-hydroperoxo model complex synthesized in the study of superoxide reductase chemistry [2]. These complexes are not side-on nor porphyrin-based but share the thiolate-ligation to the iron similar to heme-based chemistry in biological systems. (**C**) Side-on ferric-peroxo model complexes are shown to highlight differences in ligand sets.[3-4]

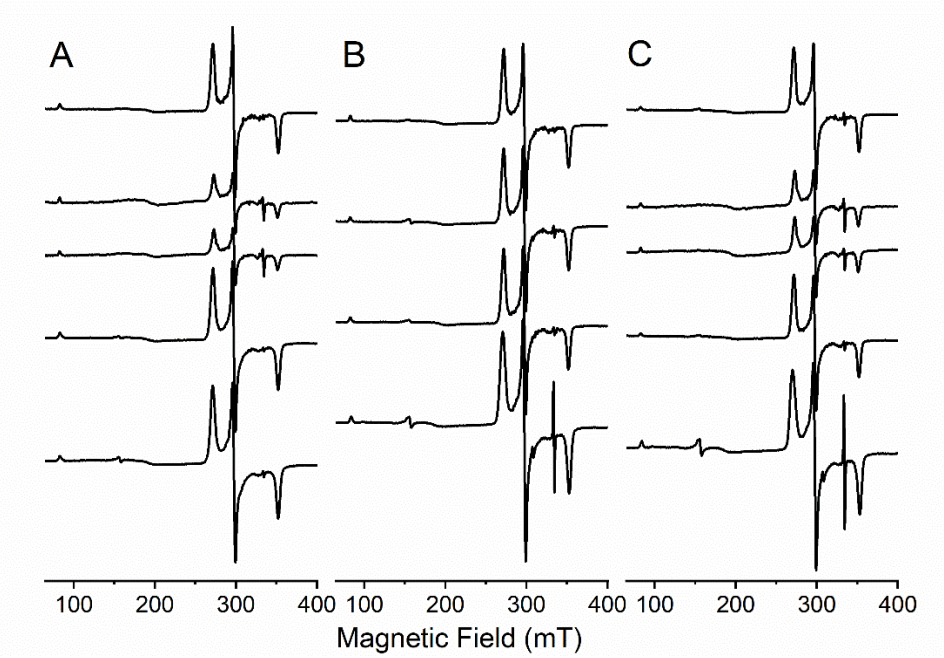

Figure S9. RFQ-EPR spectra of CYP121 ES complex reaction with 16 mM hydrogen peroxide from pH 5 – 9 at progressive time points. All time points are listed from the top spectrum to the bottom spectrum. (A) Reaction at pH 5 at time points of 0 s, 30 ms, 125 ms, 6.5 s, 20 s. (B) Reaction at pH 7.4 at time points of 0, 2, 6, and 25 s. (C) Reaction at pH 9 at time points of 0 s, 30 ms, 125 ms, 3.5 s, 25 s. In the millisecond time domain, a small radical signal was detected, which disappeared over time and a minor radical signal appeared at longer time points. The use of hydrogen peroxide as the oxidant does not result in the appearance of the high-spin species observed when using peracetic acid.

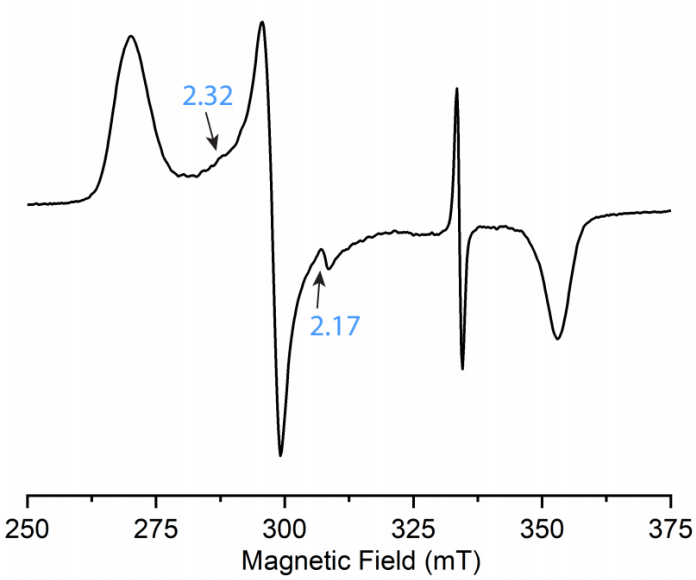

Figure S10. EPR spectra of CYP121 ES complex reaction at pH 9 with 16 mM hydrogen peroxide for 40 s. The low-spin heme is the major species, but a very minor low-spin heme that matches those captured using cryoradiolytic reduction ferric-hydroperoxo intermediates. The *g*-values of 2.32 and 2.17 match very closely to those previously reported ferric-hydroperoxo species, indicating that it is possible to generate this heme species using a high concentration of hydrogen peroxide. The long mixing time indicates that this is not an on-pathway intermediate and rather is an equilibrium species formed due to the high oxidant concentration. The spectrum was measured at 20 K using X-band (9.37 GHz), 1 mW power, 6 G modulation.

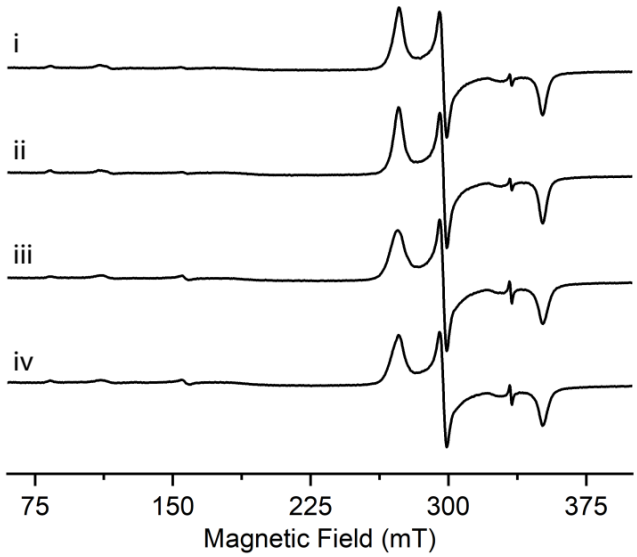

Figure S11. EPR spectra of CYP121 ES complex hand-mixed with acetic acid. The mixing time was: i) 2.5 s, ii) 3 s, iii) 5 s, and iv) 10 s. No transition from low- to high-spin heme is observed over a 10 s period. This control sample indicates that the high-spin signal is not generated due to the presence of acetic acid. The spectra were measured using X-band frequency at 20 K, 1 mW power.

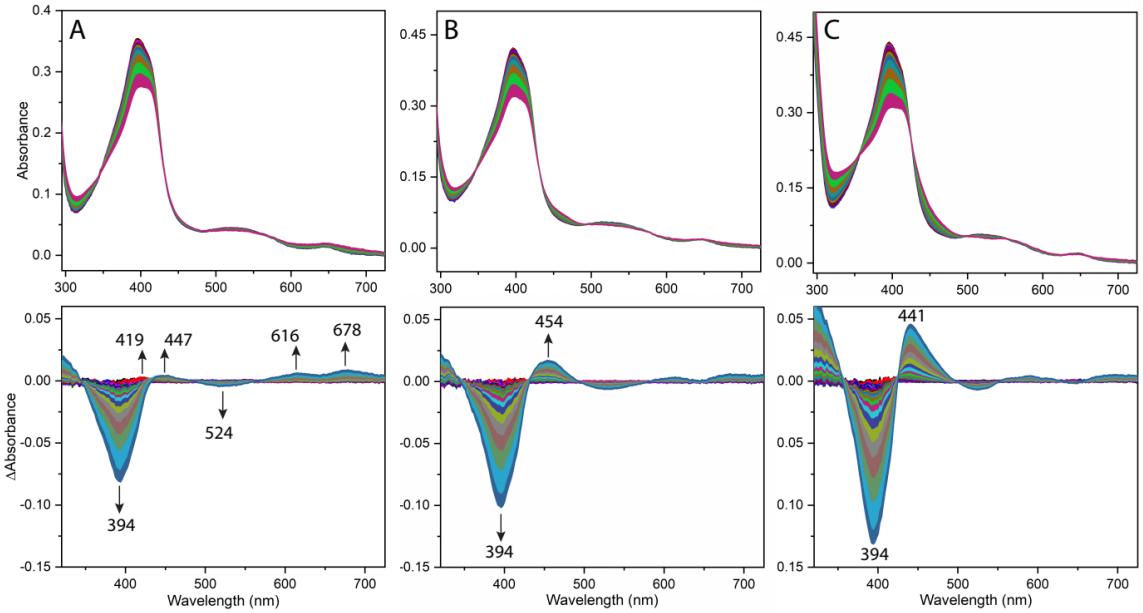

Figure S12. Stopped-flow spectroscopic analysis of the CYP121 ES complex (5 μM CYP121, 400 μM cYY final concentration) reaction with 16 mM hydrogen peroxide over a period of 60 s at A) pH 5, B) pH 7.4, and C) pH 9 with their respective difference spectrum shown below. The various transitions are reported on the difference spectra.

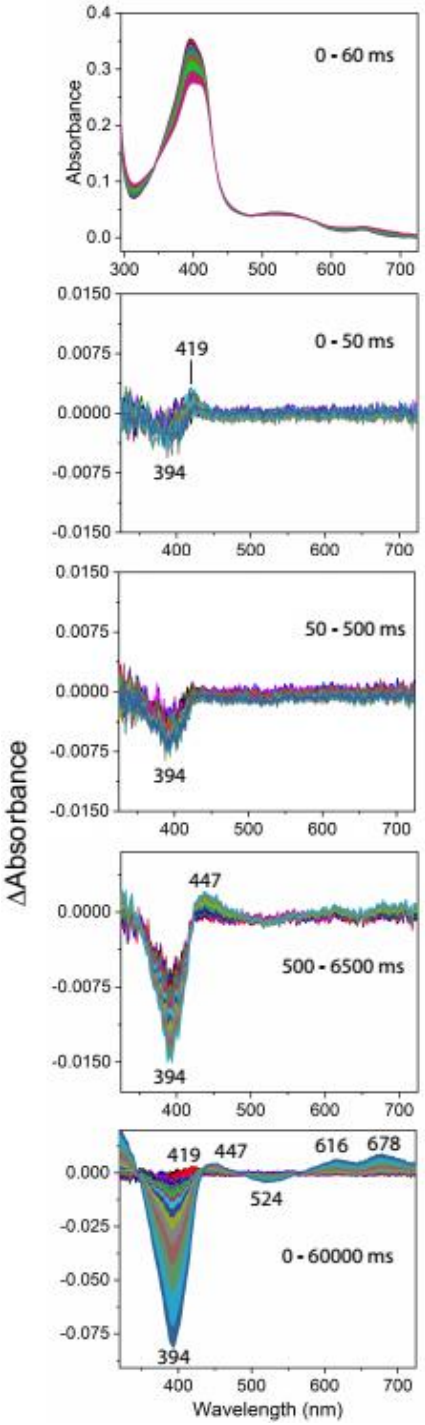

Figure S13. Stopped-flow analysis of the CYP121-cYY reaction with 16 mM hydrogen peroxide at pH 5 over a period of 60 seconds. The difference spectra at time points with distinct transitions. Within the first 50 ms, a band at 419 nm increases and decreases back to baseline concomitantly with continuous decrease of the ES Soret band at 394 nm. The ES complex Soret continually decreases through 60 s with a new band appearing at 447 nm.

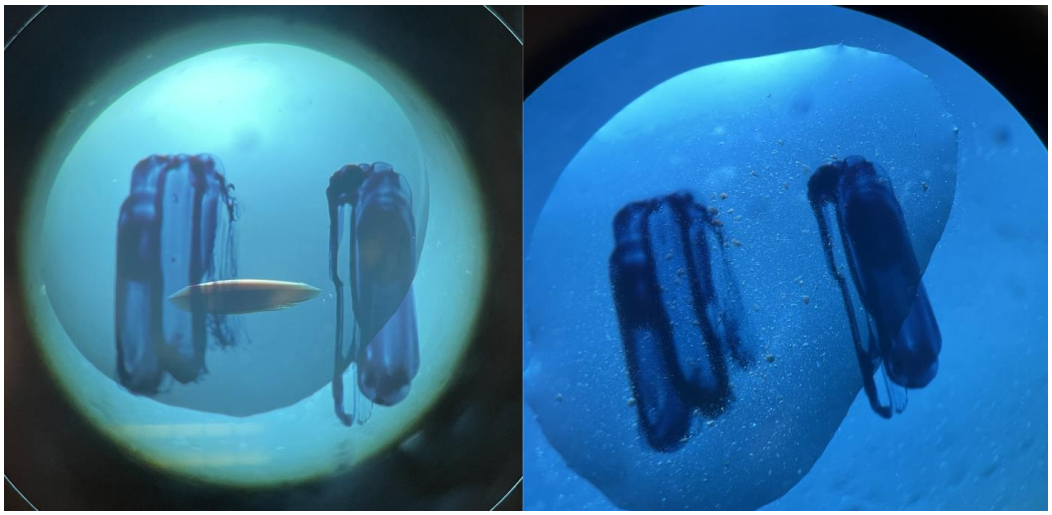

Figure S14. An image of the crystal size difference between crystals used in EPR, single-crystal UV-vis, and *in crystallo* reaction (left) and microcrystals (right). The distance between the two black markings represents ~1 mm and the images were taken at the same magnification level (40x).

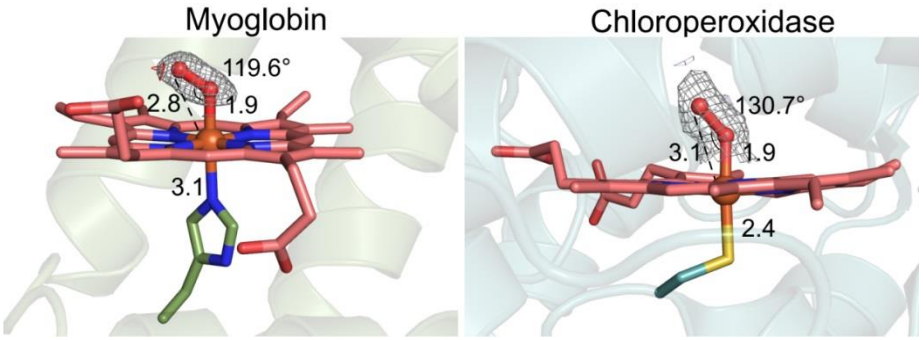

Figure S15. The ferric-hydroperoxo intermediate structures of myoglobin[5] (2Z6T.pdb) and chloroperoxidase[6] (2J5M.pdb) captured through the cryoradiolytic reduction method. Both artificially generated intermediates show an end-on binding orientation relative to the heme. Distances are measured in angstrom. The $2F_o$-F_c electron density map is contoured to 1 σ, the heme is pink, the peroxide ligand is red, and the protein-derived proximal ligand is green and teal for myoglobin and chloroperoxidase, respectively.

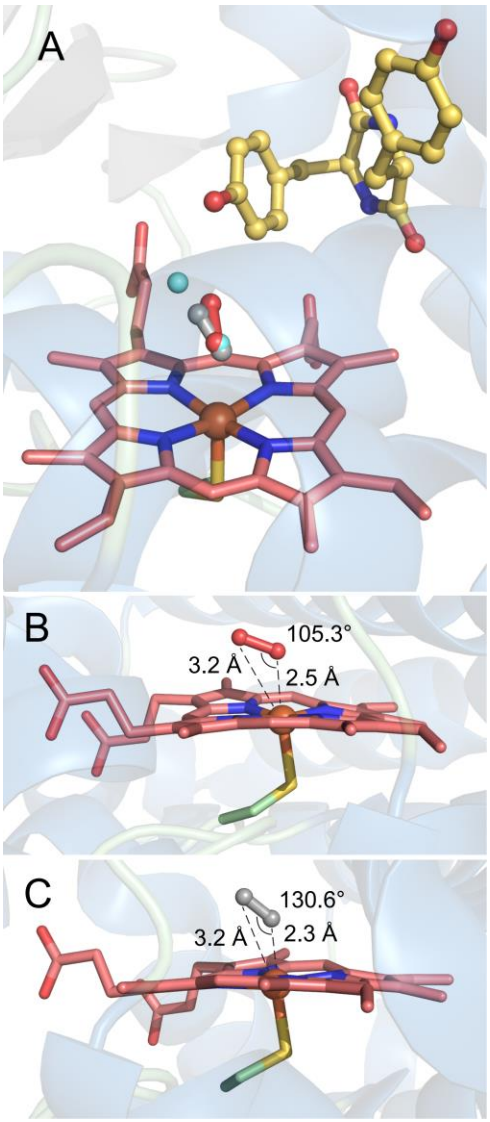

Figure S16. Comparison of CYP121 active site structure from enzyme complexed with O_2[7] (1N40.pdb), ES complex[8] (3G5H.pdb), and the cpd 0 intermediate (8TDP.pdb). (A) Overlay the three structures for direct comparison of the axial ligand to show the orientation difference between the dioxygen and peroxo/hydroperoxyl ligands and a marked positional difference compared to the second sphere water present in the ES complex. The well-ordered water molecules above the heme from the ES complex are cyan, the dioxygen adduct from the enzyme-only complex is gray, and the ferric-peroxo/hydroperoxo intermediate is red. The substrate cYY is yellow, and the heme is pink. (**B**) The measured Fe–O1, Fe–O2 distances, and Fe–O1–O2 angle for the ternary CYP121 cpd 0 structure. (**C**) The measured Fe–O1, Fe–O2 distances, and Fe–O1–O2 angle for the CYP121 enzyme only structure complexed with dioxygen. The O_2 adduct is situated in an end-on orientation as observed by the 130.6° Fe–O1–O2 coordination angle.

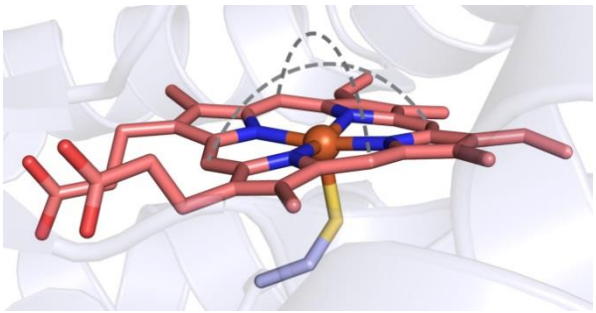

Figure S17. Heme ruffle measured in the cpd 0 intermediate structures of P450 CYP121 (8TDP.pdb). The gray dashed lines show how heme ruffle is measured. CYP121 has a very pronounced distortion of the heme (165.1° and 179.2°) compared to tyrosine hydroxylase[9] (7KQU.pdb, 175.0° and 176.0°) (*5*) and lactoperoxidase[10] (7DLQ.pdb, 170.7° and 174.0°) (*6*) measured in the same manner.

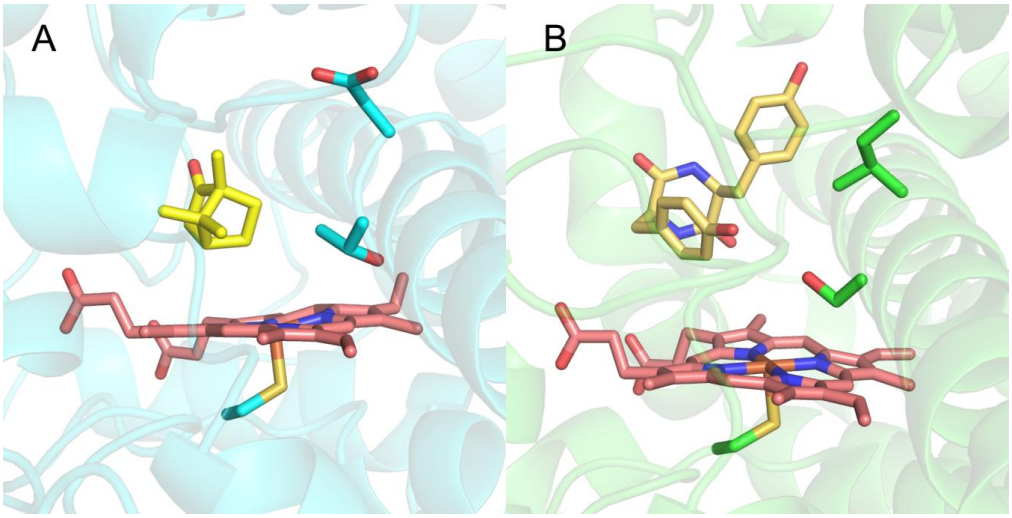

Figure S18. CYP121 does not contain active site threonine and aspartate residues that comprise the proton delivery network in hydroxylating cytochromes P450. (A) P450cam active site[11] (PDB: 5CP4) with Thr252 and Asp251 making up the proton delivery network. (B) CYP121 active site[12] (PDB: 5WP2) which has a Ser237 and Ile236 rather than a threonine and aspartate for C–C coupling.

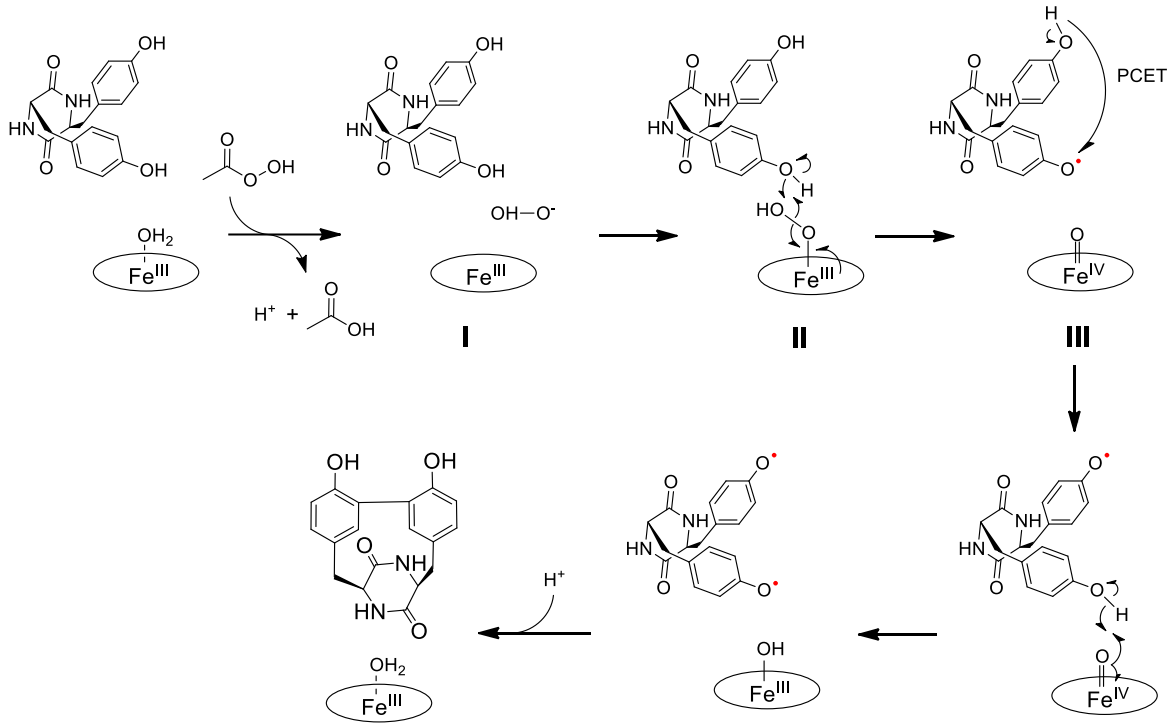

Figure S19. Proposed mechanism for C-C coupling in CYP121 using the ferric-hydroperoxo intermediate as an active oxidant. The near side-on orientation and distance from the hydroxyl proton of the cYY phenolic group facilitates hydrogen atom abstraction, removing one electron and one proton from the substrate and homolytic cleavage of the O–O bond, forming cpd II, an EPR silent species. (I) The five-coordinated ES complex is observed in the 60-s single-crystal EPR spectrum. (II) The near side-on cpd 0 intermediate is represented by the 5-ms RFQ-EPR spectrum and observed in the 120 s single-crystal EPR spectrum and the 200 ms reaction time-resolved SFX microcrystal structure. (III) The EPR silent cpd II intermediate, represented by little change from the 120 – 600 s single-crystal EPR spectrum. The substrate-based radical is rapidly quenched and not observable under *in crystallo* reaction conditions where the intended C–C coupling could not occur.

Table S1. EPR simulation parameters and relative quantification for iron species in CYP121:cYY crystals reacting with peracetic acid. EPR spectra were quantitatively simulated with the five components below. Relative amounts of each species are given for the reaction course with peracetic acid.

	LS	HS_{5c}	HS_{6c}[a]	HS_{6c}[b]	$HS_{4.3}$
S	1/2	5/2	5/2	5/2	5/2
g values	2.46, 2.25, 1.90	8.09, 3.49, 2.19	5.76, 2.00	6.42, 5.49, 1.99	4.27, 2.00
g strain	0.03, 0.19, 0.016	0.20, 0.07, 0.11	0.10, 0.10, 0.01	0.14, 0.13, 0.02	0.03, 0.10, 0.04
D	-	20	9.4	9.4	0.64
E/*D*	-	0.108	0.0005	0.0184	0.325
ES	0.67	0.31	0.01	< 0.01	< 0.01
30 s	0.42	0.22	0.34	0.03	< 0.01
60 s	0.19	0.12	0.59	0.09	< 0.01
120 s	0.10	0.06	0.65	0.19	< 0.01

Table S2. Comparison of Fe–S, Fe–O1, and Fe–O2 bond lengths in the enzyme only, ES complex, tr-SFX-XFEL structure of ES complex, and tr-SFX-XFEL structure of ES complex reacting with oxidant for 200 ms. The Fe–O1 distance for the tr-SFX reaction structure does not significantly differ from the distances of other reported CYP121 structures.

CYP121 structures	Fe–S (Å)	Fe–O1 (Å)	Fe–O2 (Å)	PDB entry
E only	2.35	2.47	-	3G5F
E-O_2	2.38	2.25	3.18	1N40
ES	2.35	2.44	-	3G5H
SFX ES	2.31	2.44	-	8TDQ
SFX ES 200 ms	2.27	2.54	3.22	8TDP

Table S3. Cytochrome P450 structures chosen for comparison of active site architecture to CYP121

CYP51, 1E9X.pdb	P450nor, 1EHE.pdb	CYP119, 1F4U.pdb	CYP102A1, 1FAG.pdb
P450eryF, 1JIN.pdb	OxyB, 1LFK.pdb	CYP2C9, 1OG5.pdb	P450 2B4, 1PO5.pdb
OxyC, 1UED.pdb	P450 3A4, 1W0F.pdb	CYP19A1, 3EQM.pdb	CYP101, 2ZWT.pdb
CYP17A1, 3RUK.pdb	P450 2E1, 3T3Z.pdb	CYP105AS1, 4OQR.pdb	TxtC, 6F0C.pdb
StvP2, 6M4Q.pdb	CYP102L1, 6N6Q.pdb	P450 21A2, 4Y8W.pdb	CYP2A6, 3T3R.pdb

References

1. Dornevil, K.; Davis, I.; Fielding, A. J.; Terrell, J. R.; Liu, A., Crosslinking of dicyclotyrosine by the cytochrome P450 enzyme CYP121 from *Mycobacterium tuberculosis* proceeds through a catalytic shunt pathway. *J. Biol. Chem.* **2017,** *292*(33), 13645-13657.
2. Namuswe, F.; Kasper, G. D.; Sarjeant, A. N.; Hayashi, T.; Krest, C. M.; Green, M. T.; Moënne-Loccoz, P.; Goldberg, D. P., Rational tuning of the thiolate donor in model complexes of superoxide reductase: Direct evidence for a *trans* influence in FeIII−OOR complexes. *J. Am. Chem. Soc.* **2008,** *130*(43), 14189-14200.
3. Burstyn, J. N.; Roe, J. A.; Miksztal, A. R.; Shaevitz, B. A.; Lang, G.; Valentine, J. S., Magnetic and spectroscopic characterization of an iron porphyrin peroxide complex. Peroxoferrioctaethylporphyrin (1-). *J. Am. Chem. Soc.* **1988,** *110*(5), 1382-1388.
4. Liu, J. G.; Ohta, T.; Yamaguchi, S.; Ogura, T.; Sakamoto, S.; Maeda, Y.; Naruta, Y., Spectroscopic characterization of a hydroperoxo-heme intermediate: conversion of a side-on peroxo to an end-on hydroperoxo complex. *Angew. Chem. Int. Ed.* **2009,** *48*(49), 9262-9267.
5. Unno, M.; Chen, H.; Kusama, S.; Shaik, S.; Ikeda-Saito, M., Structural characterization of the fleeting ferric peroxo species in myoglobin: Experiment and theory. *J. Am. Chem. Soc.* **2007,** *129*(44), 13394-13395.
6. Kühnel, K.; Derat, E.; Terner, J.; Shaik, S.; Schlichting, I., Structure and quantum chemical characterization of chloroperoxidase compound 0, a common reaction intermediate of diverse heme enzymes. *Proc. Natl. Acad. Sci. U.S.A.* **2007,** *104*(1), 99-104.
7. Leys, D.; Mowat, C. G.; McLean, K. J.; Richmond, A.; Chapman, S. K.; Walkinshaw, M. D.; Munro, A. W., Atomic structure of *Mycobacterium tuberculosis* CYP121 to 1.06 reveals novel features of cytochrome P450 *J. Biol. Chem.* **2003,** *278*(7), 5141-5147.
8. Belin, P.; Le Du, M. H.; Fielding, A.; Lequin, O.; Jacquet, M.; Charbonnier, J. B.; Lecoq, A.; Thai, R.; Courçon, M.; Masson, C.; Dugave, C.; Genet, R.; Pernodet, J. L.; Gondry, M., Identification and structural basis of the reaction catalyzed by CYP121, an essential cytochrome P450 in *Mycobacterium tuberculosis*. *Proc. Natl. Acad. Sci. U.S.A.* **2009,** *106*(18), 7426-7431.
9. Wang, Y.; Davis, I.; Shin, I.; Xu, H.; Liu, A., Molecular rationale for partitioning between C-H and C-F bond activation in heme-dependent tyrosine hydroxylase. *J. Am. Chem. Soc.* **2021,** *143*(12), 4680-4693.
10. Singh, P. K.; Sharma, P.; Bhushan, A.; Kaur, P.; Sharma, S.; Singh, T. P., Structure of a ternary complex of lactoperoxidase with iodide and hydrogen peroxide at 1.77 Å resolution. *J. Inorg. Biochem.* **2021,** *220*, 111461-111469.
11. Vidakovic, M.; Sligar, S. G.; Li, H.; Poulos, T. L., Understanding the role of the essential Asp251 in cytochrome P450cam using site-directed mutagenesis, crystallography, and kinetic solvent isotope effect. *Biochemistry* **1998,** *37*(26), 9211-9219.
12. Fielding, A. J.; Dornevil, K.; Ma, L.; Davis, I.; Liu, A., Probing ligand exchange in the P450 enzyme CYP121 from *Mycobacterium tuberculosis*: Dynamic equilibrium of the distal heme ligand as a function of pH and temperature. *J. Am. Chem. Soc.* **2017,** *139*(48), 17484-17499.